River Water Treatment in Chennai: Producing Drinking Water by Reverse Osmosis and Biocrude Oil by Hydrothermal Liquefaction

A Technical Report submitted to the Department of Chemical Engineering

Presented to the Faculty of the School of Engineering and Applied Science

University of Virginia • Charlottesville, Virginia

In Partial Fulfillment of the Requirements for the Degree

Bachelor of Science, School of Engineering

Natalie Thomas

Spring, 2022

Technical Project Team Members
Jacob Gendron
Chris Hawkins
Katarina Liddell
Abhilash Mangu

On my honor as a University Student, I have neither given nor received unauthorized aid on this assignment as defined by the Honor Guidelines for Thesis-Related Assignments

Advisor

Eric Anderson, Department of Chemical Engineering

Technical Report

Table of Contents

1. Executive Summary

This paper describes the design of a reverse osmosis (RO) water treatment plant located in Chennai, India. The plant is designed to intake 13,300 m^3 of water from the Cooum River to provide 10,052 m^3 of clean drinking water to Chennai every day. The level of production is expected to accommodate the water needs of approximately 230,000 people every day or 1% of the city's daily water needs. The process also takes advantage of the sewage and solid wastes in the Cooum River to produce a bio-crude oil via a hydrothermal liquefaction (HTL) reactor. This bio-crude oil will help power a percentage of the plant, reducing operating costs.

Chennai, India, relies on rain during the monsoon season to supply the city with clean water. However, these rain patterns recently have become increasingly unreliable, leading to extensive water scarcity (Varadhan, 2019). The following project aims to design a drinking water treatment plant on the Cooum River to provide a source of clean drinking water for the city, simultaneously addressing water scarcity and reducing the extensive pollution of the river. A drinking water treatment plant using the Cooum River as a source of water, as opposed to rainfall, would provide a consistent and cheap source of drinking water to Chennai to support the city's growth.

Approximately 13,300 m^3/day is pumped from the Cooum River through a screen, collecting larger solids for HTL, and sending water and smaller suspended particles to sedimentation. A series of sedimentation tanks removes 86% of all particulates from the water. The bottoms of the sedimentation tanks will be transferred to HTL, and the overflow is sent to microfiltration for further processing.

The microfilters remove all suspended solids and greatly reduce the amounts of biological oxygen demand (BOD) and chemical oxygen demand (COD). Twenty four microfiltration modules placed in parallel will be used to achieve a permeate stream of 12,672 m^3/day of water which flows to the RO membranes. Three stages of RO sufficiently clean the water to Indian Standard Drinking Water Specifications (Bhavan, 2012). The permeate water from each stage is collected and treated by ultraviolet (UV) light. UV treatment eliminates total coliform bacteria and any remaining viruses or protozoa. The RO process has an overall recovery of about 79%, producing a permeate flow of 10,052 m^3/day. The retentate flow rate from stage 3 is 2,620 m^3/day which is pumped into the Bay of Bengal as waste.

To supplement the high energy usage of reverse osmosis, a hydrothermal liquefaction reaction will be carried out using the wet solid wastes collected from screening, sedimentation, and microfiltration. A 10 m^3 isothermal, baffled, batch reactor will carry out one 3 hour batch a day of 5.2 m^3 of wet solids. The reactor will operate at a temperature of 300^{o}C and a pressure of 25MPa. The reaction produces water, char, bio-crude oil, and gases. In order to prevent the reactor system from overpressurizing, 10% of the reactor contents will be cycled through a 5 MPa flash drum every minute to vent the gases formed during the reaction. A shell and tube heat exchanger will conserve heat lost from the stream leaving to the flash drum and transfer it back to the stream re-entering the reactor.

A decanter is used to separate the water from the char and oil which will both be sent to an agitated holding tank. The wastewater from the reaction is pumped to the microfiltration system for further purification. The mixture of oil and char will be fed to a boiler to produce superheated steam. The steam will flow through a turbine, generating approximately 301 kW

hours of energy per batch that can be sustained for a year, supplementing approximately half of the energy required by RO per day.

The total capital investment to realize these designs is estimated to be approximately $263 million. About 69% of this capital cost can be attributed to reverse osmosis and microfiltration, and about 17% is attributed to HTL. The operating costs of running the plant are approximately $162 million per year, including the raw materials, utilities, labor, and the fixed capital investment (FCI). The drinking water produced will be sold at 10 cents per liter, providing an estimated revenue of $367 million per year. After a cash flow analysis, the internal rate of return on our investment is approximately 39%. In addition to the economic benefits, the following design provides significant social and environmental benefits to Chennai, with a minimal risk to the safety of the plant workers. Taking these benefits into consideration, the conclusion of this report is that the following design is an overall benefit to the community of Chennai and should be moved forward to construction. It is recommended that before implementing this design, a more detailed investigation into the Cooum River's contaminants is completed over the course of a year. Additionally, larger scale research of the HTL reaction should be conducted to ensure a safe and successful reactor system.

2. Introduction

2.1 Background and Motivation

Chennai, India, has faced severe water scarcity due to abnormal rain patterns and the pollution of local water sources. Three large rivers run through Chennai, which in the distant past were used as sources of clean water to the area (Agoramoorthy, 2014). Discharge of industrial and agricultural waste over decades has caused the rivers to be heavily polluted and currently incapable of sustaining life. Pollutants in the rivers of Chennai consist primarily of sewage, trash, industrial effluent, salts and heavy metals (Elangovan and Dharmendirakumar, 2013). As a result of the polluted surface water and diminished groundwater supply, Chennai relies on rain during the monsoon season to supply the city with clean water. Recently, these rain patterns have become increasingly unreliable, leading government officials to declare “Day Zero" in June 2019, the day on which the city’s four reservoirs ran dry (Varadhan, 2019).

Chennai was the fourth largest city in India in 2011 according to census data, and has recently experienced an “explosive” growth in population due to recent developments in the industrial, health, and education sectors. Despite these advancements, there are still many areas in the city that do not have access to clean water, particularly in slums where there is limited access to all basic amenities (Krishnamurthy & Desouza, 2015). The population of the city has grown to over 11 million since 2011, and the number of people living in slums is increasing proportionally (Chennai Population, 2021).

It is estimated that only 30% of municipal sewage undergoes proper treatment in Chennai, with the rest being dumped into its rivers (Agoramoorthy, 2014). Furthermore, 30% of the municipal drinking water fails quality tests, with high bacteria and salt levels (TOI, 2019).

When available, much of the population relies on water from the city's reservoirs. Periods of drought lead people to turn to bottled water or privately owned water trucks as the reservoir supply dwindles. However, packaged water prices are exceedingly high in relation to the average household income and not everyone can afford the luxury of clean water. The following project aims to design a drinking water treatment plant on Chennai's biggest river, the Cooum, to provide a source of clean drinking water for the city, simultaneously addressing water scarcity and reducing the extensive pollution of the river. A drinking water treatment plant using the Cooum River as a source of water, as opposed to rainfall, would provide a consistent and cheap source of drinking water to Chennai to support the city's growth.

In designing this water treatment plant, two periods or design cases were considered and are referenced as operating seasons throughout the design description. These two periods are "pre-monsoon" and "post-monsoon" seasons. Monsoon season is typically from June to September (Halpert and Bell, n.d.), and reports for pre-monsoon concentrations of contaminants in river water are typically taken in the month of June (Chennai Rivers Restoration Trust, 2020). Therefore, it was decided that the pre-monsoon season would be considered all days from January 1st to July 1st (181 days) and the post-monsoon season would be considered all days from July 1st to January 1st of the following year (184 days). The extra day from a leap year was neglected.

2.2 Previous Work

The design discussed here involves two major aspects: removal of pollutants from river water, and the processing of wet biomass into a useful product. Eichorn et al. outlines various separations techniques that are commonly used in drinking water treatment, which helped us to determine which of these processes to use in our design (2009). These include sedimentation and microfiltration (Central Pollution Control Board, Ministry of Environment and Forests, n.d.). Additionally, reverse osmosis is included as a common feature in all water treatment operations to remove small particles that microfiltration cannot. Eichorn et al. also includes a final disinfection stage to provide residual protection from contaminants after purification (2009).

The design for the sedimentation tank was largely inspired by a combination of novel modeling techniques from Cyprus International University and the University of Sydney, and design specifications published in the Journal of Environmental Engineering (Riazi et al., 2020; Swamee & Tyagi, 1996). One study by Bhattacharya et al. looked into the use of both microfiltration and reverse osmosis in the treatment of dirty industrial effluent water (2013). Due to the success of tubular microfiltration units with crossflow microfiltration in the design presented in this study, a similar configuration was used for the current design. Bhattacharya et al. also used spiral wound polyamide membranes for reverse osmosis and explained how an acidic solution was used to clean the membranes when they were not under operation (2013). As a result, the same type of membranes and a similar cleaning procedure were included in the current design. Lastly, UV treatment follows industry standards for Class A systems, which are the strongest disinfection systems on the market and eliminate all pathogens (ESP Water Products, n.d.).

Hydrothermal liquefaction is a novel process that has never been attempted on a large scale. Given the large amounts of sewage and other pollutants present in the river, as indicated by Gowri et al. (2007), the implementation of hydrothermal liquefaction is theoretically advantageous. The study by Rosendahl et al. provided the reaction conditions necessary for the process (2018). Information about the products of HTL and how the product is affected by the reactor feed composition was researched by Ramirez et al. (2015) as well as Cheng et al. (2020). The research of these two groups established the foundations for many assumptions made regarding HTL. Professor Lisa Colosi-Peterson was also an extremely helpful resource for answering questions regarding the progress of HTL research and prior existing knowledge in the field.

3. Process Flow Diagram

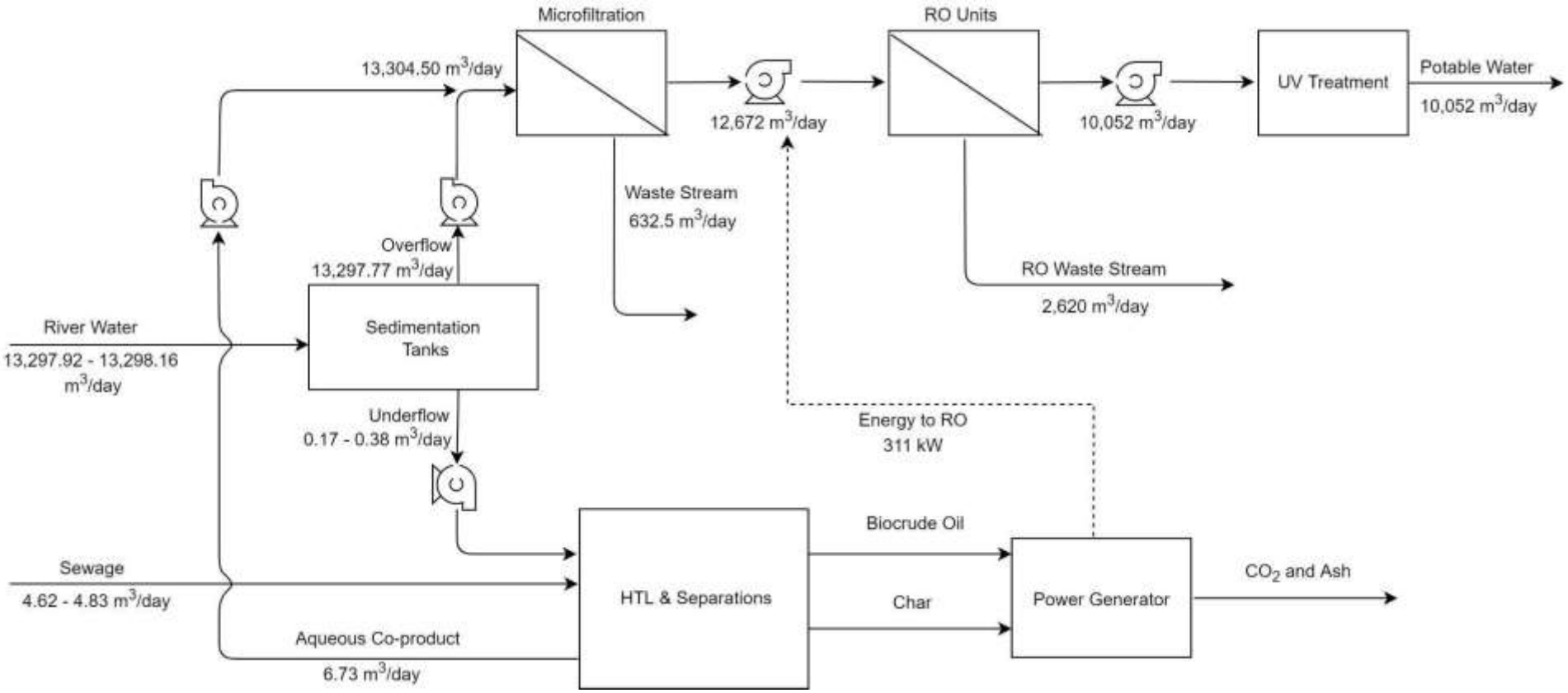

Figure 3.1 Overall process flow diagram, where volumetric water intake, sewage intake, and underflow change pre and post monsoon.

4. Pre-Screening

4.1 Introduction

The water treatment plant has multiple pumps and other equipment that could be damaged by solids or debris that are not expected to be in the water. Debris consists of twigs, leaves, and any garbage or plastics that could float in the river water (US EPA, 2003). Debris can also affect the effectiveness of sedimentation and in turn reduce the efficiency of our filtration processes. To prevent any damage to our equipment and maintain an efficient process, the water must be screened to remove this debris before entering the sedimentation pond.

The screen in our process will be a Raptor® FalconRake® Bar Screen. The screen operates by allowing water to flow through the screen, while trapping any large solids and debris on the screen. The debris is mechanically raked up the screen where it is then dumped in a collection bin. This process is depicted in Figure 4.1.1 below. The collected debris will consequently be transported to the HTL reactor as part of its feed.

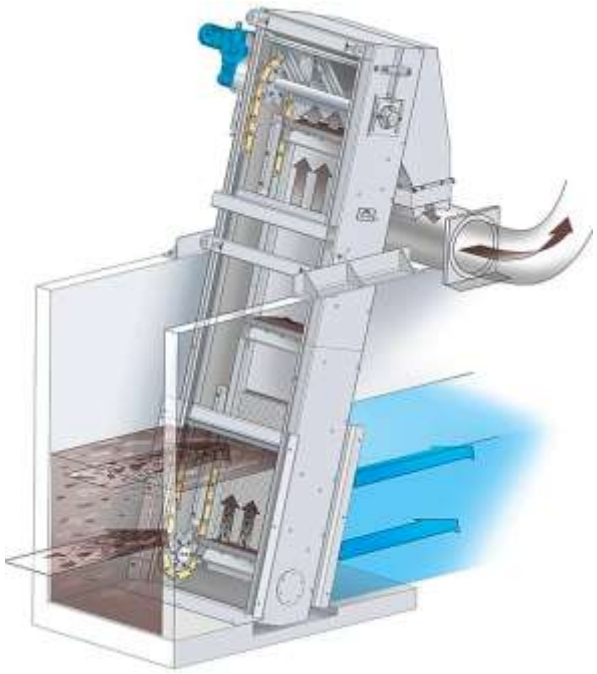

Figure 4.1.1 Mechanically cleaned bar screen diagram. (Huber, 2022)

4.2 Bar Screen Design

The Raptor® FalconRake® Bar Screen will have 6 mm spaces between each bar with bar widths and depths of 10 and 30 mm respectively (US EPA, 2003). The screen slope will be 15 degrees from vertical. The water will flow at an approach velocity of around 0.25 m/s. This slow approach velocity will result in a screening capture of 93% (MBR Screening, 2021). Due to the variability in the amount of debris in the water from day to day, the screen will be able to separate up to 0.136 m^3/day of debris (US EPA, 2003).

The screen is mechanically cleaned with multiple rakes and has a lifting capacity of 1000 lbs. The bars are made out of standard stainless steel which will reduce corrosion. The motor that powers the rakes operates at low horsepower making it economically viable and energy efficient (Raptor, 2020).

The inlet from the river to the bar screen will be 13,300 m^3/day. At an approach velocity of 0.25 m/s, the bar screen will be 1.0 m across and submerged in 0.62 m of the river water to screen all of the water in a given day. All debris collected from the screen will be transported to the HTL reactor as feed.

5. Sedimentation

5.1 Introduction

After large waste has been filtered out with the bar screen, the water travels through a series of sedimentation tanks to filter out settleable and suspended solids. Sedimentation is frequently used in both drinking water treatment plants and wastewater treatment plants to reduce the total suspended solid (TSS) concentration of the water. The process uses large tanks and slow-moving flows that allow gravity to pull heavier particles to the bottom of the tank (*Sedimentation*, n.d.). Over time, these sediments form a thick sludge layer that can be manually or mechanically scraped out and discarded (Bache & Gregory, 2021). Though sedimentation is time consuming, several factors make this process extremely beneficial. As opposed to similar processes, such as flocculation and coagulation, sedimentation does not require the addition of chemicals. This absence of additional chemicals lowers operating costs and eliminates the need for additional removal steps later on (Bache & Gregory, 2021). Moreover, sedimentation makes subsequent processing easier by decreasing the variation in water quality and protecting the filters used later in the process.

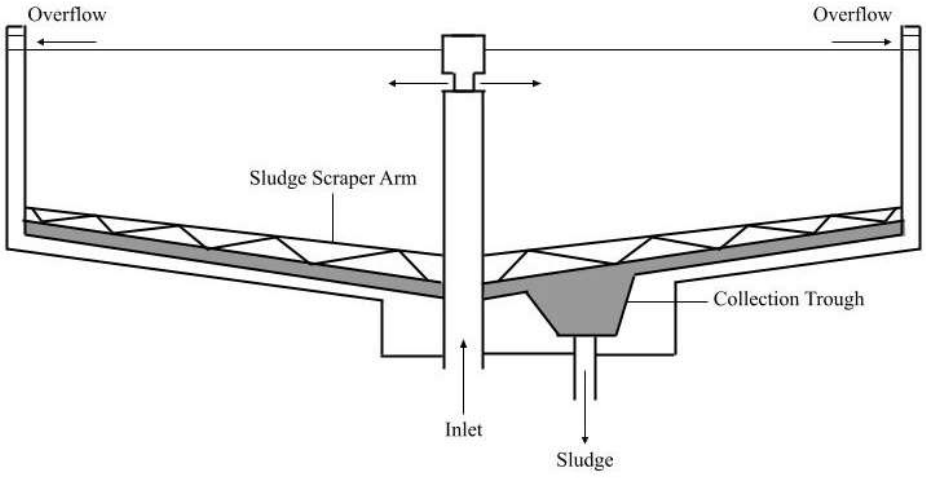

Figure 5.1.1 Side view of the circular sedimentation tank, with a central inlet and mechanical sludge scrapers.

Within the water treatment industry, there are many designs for sedimentation systems depending on water flow, TSS concentration, and the intended product. In the United States, circular tanks, as shown above in Figure 5.1.1, are the most commonly used design, because they can process the same volume of flow while taking up less land than other methods (Bache & Gregory, 2021). However, rectangular tanks with horizontal flows, such as the tank depicted in Figure 5.1.2, are typically more efficient at particle removal (Bache & Gregory, 2021). To achieve the best TSS removal rates, while taking into account the area of land required for construction, the final sedimentation design utilizes two circular tanks and one rectangular tank.

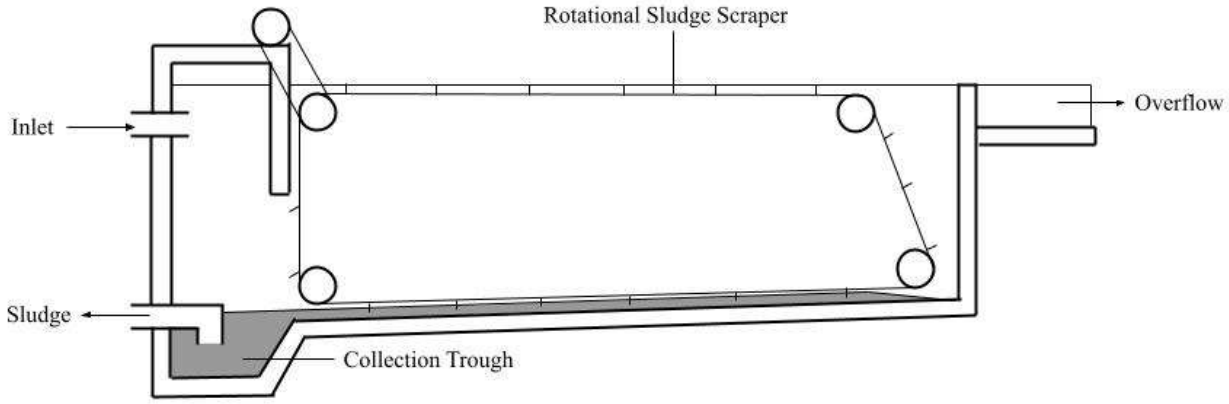

Figure 5.1.2 Side view of the rectangular sedimentation tank, with a mechanical scraping system and sump pump collection.

5.2 Overall Design and Material Balances

Sedimentation design varies largely depending on the condition of the feed and intended effluent. The defining characteristics of sedimentation include the concentration of suspended solids and the presence of a flocculent. The TSS concentration in the Cooum River is considered dilute as it is always below the 500 mg/L cutoff for dilute sedimentation (British Columbia Ministry of Environment, 2016). As noted in Table 5.2.1, the incoming feed has 49.30 and 22.75 mg/L for pre-monsoon and post-monsoon season, respectively (Elangovan, 2013). The addition of a chemical flocculant or coagulant will require additional processing to remove any residuals left in the overflow. To minimize processing and cost, flocculation will be omitted. Therefore, the river water will undergo dilute, non-flocculant, free-settling sedimentation.

While the average TSS concentrations are below 500 mg/L, historically there have been several large precipitation events annually in Chennai, especially during the monsoon season. Additionally, because of the presence of poorly regulated industry upstream, there is a risk of

extreme contamination of the river. To ensure that the plant can handle large fluctuations of both flow and contaminant concentration, two rounds of sedimentation are used. The difference in TSS content between these two stages can be seen in Table 5.2.1 in “Overflow 1” and “Overflow 2”. Using two stages allows for an additional 32% sludge collection by volume per day.

After pre-screening, the river water will flow into a circular, radial flow tank. The overflow from this preliminary tank will continue to a rectangular, horizontal flow tank for further processing. The final overflow will move forward to microfiltration. The underflow, or sludge, collected in the tanks will be mechanically scraped out and sent to the HTL reactor. This process is detailed in the sedimentation process flow diagram, Figure 5.1.3, below.

As per industry standard, the circular sedimentation tanks will be constructed as a pair, operating alternately (Voutchkov, 2005). Because these tanks will take in the most contaminated water, they run the risk of accumulating excessive sediment or encountering larger contaminants. In the event that one tank must be taken out of operation for maintenance, the second tank allows production to continue (Voutchkov, 2005). The rectangular sedimentation tank does not face this potential risk and therefore will be constructed as a singular unit.

Table 5.2.1 Sedimentation stream balances for pre/post monsoon season, where "1" refers to streams exiting the radial flow tanks and "2" refers to streams exiting the horizontal flow tank.

Pre-monsoon Balances			Post-monsoon Balances		
Stream	TSS Conc. (mg/L)	Vol. Flow (m^3/day)	Stream	TSS Conc. (mg/L)	Vol. Flow (m^3/day)
Feed	49.30	13,297.92	Feed	22.75	13,298.16
Overflow 1	19.72	13,297.66	Overflow 1	9.10	13,298.04
Overflow 2	6.90	13,297.55	Overflow 2	3.19	13,297.99
Stream	Solids Mass Flow (kg/day)	Vol. Flow (m^3/day)	Stream	Solids Mass Flow (kg/day)	Vol. Flow (m^3/day)
Underflow 1	393.35	0.26	Underflow 1	181.51	0.12
Underflow 2	170.45	0.11	Underflow 2	78.66	0.05
Total to HTL	563.81	0.38	Total to HTL	260.18	0.17

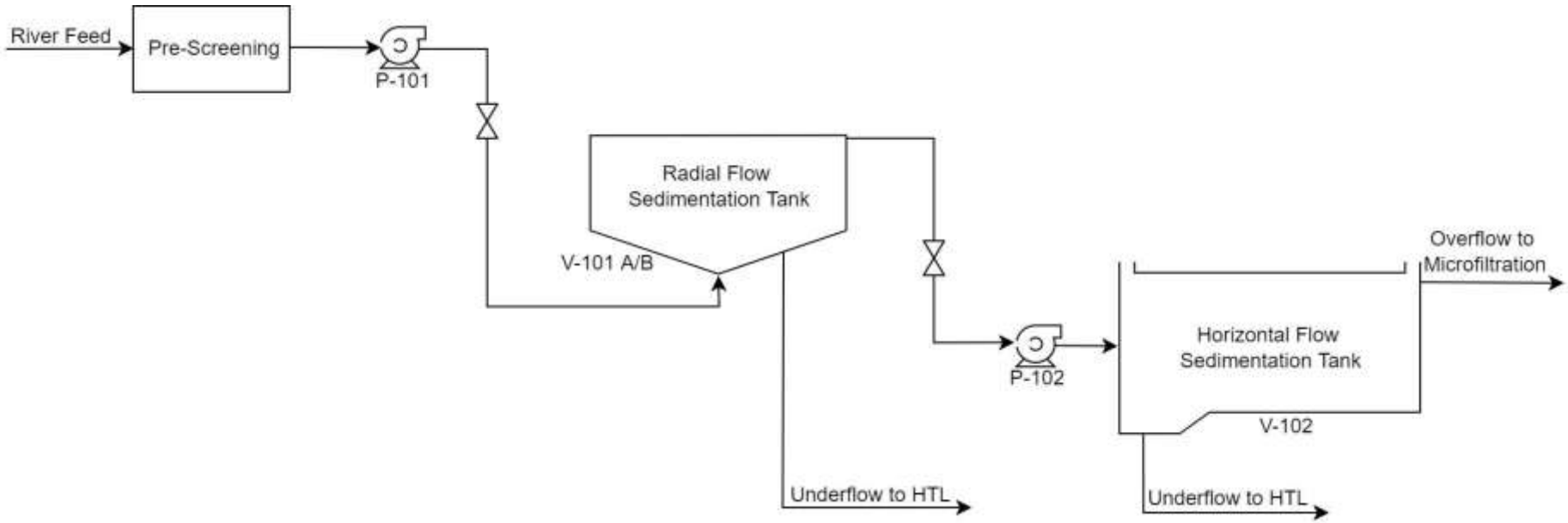

Figure 5.1.3 Process flow diagram of the sedimentation system, showing pre-screening, parallel radial flow clarifiers, and a horizontal flow clarifier.

5.3 Feed Characteristics and Settling Velocities

To calculate the size of the settling tanks, the duration of settling, and the suspended solids removal rate, the characteristics of the TSS in the river must be known. However, this information is not readily available and continuation of this project requires on-site testing of the particulates in the Cooum River to verify the validity of the following calculations.

According to several sources, the anthropogenic contributions to waste in the Cooum River involve mainly plastics, glass, and sewage (Ganapathy et al., 2021; Ramakrishnan & Lakshmi, 2019; Raman, 2019). Additionally, the bed of the river is made up largely of loose sandy soils (Anirudhan & Ramaswamy, 2009). To determine the necessary detention time within the sedimentation tanks, the settling velocities of the particulates was calculated. More specifically, the settling velocity for sand, polyester, nylon, poly(methyl methacrylate) (PMMA), polystyrene (PS), glass, and sewage was determined. The particular plastics evaluated were based both on the most frequently used plastics in India, and on a study conducted on the distribution of microplastics in the Kosasthalaiyar River and the Adyar River - the two other large rivers in Chennai (Ganapathy et al., 2021).

To account for the irregularity of the particles within the river, the calculations used an ellipsoidal model developed in collaboration between Cyprus International University and the University of Sydney (Riazi et al., 2020). The model was initially developed for improved drag coefficients and settling velocities for carbonate sands, and was adapted to fit the parameters of the particles in the river. Equation (5.3.1) was used to determine the settling velocity of the particles

$$\omega^2 = \frac{11}{15}\frac{(S-1)g}{C_D}S_f^{\frac{2}{3}}d_n \quad (5.3.1)$$

where ω is the settling velocity, S is the specific gravity of the sediment particle, g is the gravitational acceleration, C_D is the drag coefficient, S_f is the Corey Shape factor, and d_n is the nominal diameter of the particle. The drag coefficient and the shape factor of the particles were determined using (5.3.2) and (5.3.3), respectively.

$$C_D = (\frac{a_1 * \nu}{d_n^{1.5} * g^{0.5}} + a_2)^{a_3} \quad (5.3.2)$$

where a_1, a_2, and a_3 are shape dependent constants experimentally calibrated in the research paper and used as estimations in calculations for the particles in the Cooum River, and ν is fluid kinematic viscosity.

$$S_f = \frac{d_s}{\sqrt{d_l * d_i}} \quad (5.3.3)$$

where d_l, d_i, and d_s are the longest, intermediate, and shortest diameters of the particles. Using the aforementioned sources to determine the composition of solids in the river, the average sizes for such particulates was found using available literature and the settling velocities were calculated accordingly (Ganapathy et al., 2021). To account for size variation among particles, the smallest and largest sizes typically found in the river were used in calculations to determine the impact of size on settling velocity. The settling velocities for the larger particles were much

greater than sedimentation tank flows and were omitted in future calculations. Additionally, the average water temperature of the Cooum River throughout the year is 28.5 °C (Dhamodharan et al., 2016). At this temperature the kinematic viscosity of water is $8.26*10^{-7}$ m^2/s. The settling velocities for the particles in the river can be seen in Table 5.3.1, below.

Table 5.3.1 Nominal diameter, specific gravity, and settling velocity for particles in the Cooum River.

Sediment Type	Nominal Diameter (m)	Specific Gravity	Settling Velocity (m/d)
Sand Grains	9.0×10^{-5}	1.50	56.07
Polyester Fibers	9.0×10^{-5}	1.38	48.88
Nylon Fibers	9.0×10^{-5}	1.14	29.67
PMMA Fragments	9.0×10^{-5}	1.18	33.64
PS Fragments	2.1×10^{-4}	1.05	30.04
Sewage Sludge	2.0×10^{-4}	1.03	39.57
Glass Fragments	9.0×10^{-5}	2.50	97.12

Overall, the microplastics have the lowest settling velocities. Nylon, frequently found in the form of fibers shed from fabric, has the slowest settling velocity out of the particles surveyed: 29.67 m/day. This value was used as a barrier when designing the sedimentation tanks. The velocity of the flow must consistently be lower than 29.67 m/day to avoid excessive amounts of suspended particles moving to microfiltration. This eliminates potential problems of buildup and limited required maintenance of the microfilters.

5.4 Tank Design and Dimensions

The design of the sedimentation tanks relied heavily on standard values cited in literature. Parameters such as basin depth and surface overflow rate were chosen based on the average values in available literature resources. These values were then used as a basis to calculate the remaining parameters for each tank. Per several sources, the depth of a mechanically separated tank should be larger than 3.5 m, but smaller than 6 m to avoid excessive construction costs (MECC, n.d.; Scholz, 2015). Because the river water is dilute in regards to TSS, a depth of 4 m was used for calculations. This meets industry standards and minimizes construction costs. The preliminary depth measurement does not include the allowance for the sludge layer or headspace at the top of the tank. The final depths of the circular and rectangular tanks, as well as widths and floor slopes, can be seen on Figure 5.4.1 and Figure 5.4.2, respectively. As for the surface loading rate, the standard range given for free-settling tanks is 16-32 $m^3/(day*m^2)$, with the typical rate being 24 $m^3/(day*m^2)$ (Scholz, 2015).

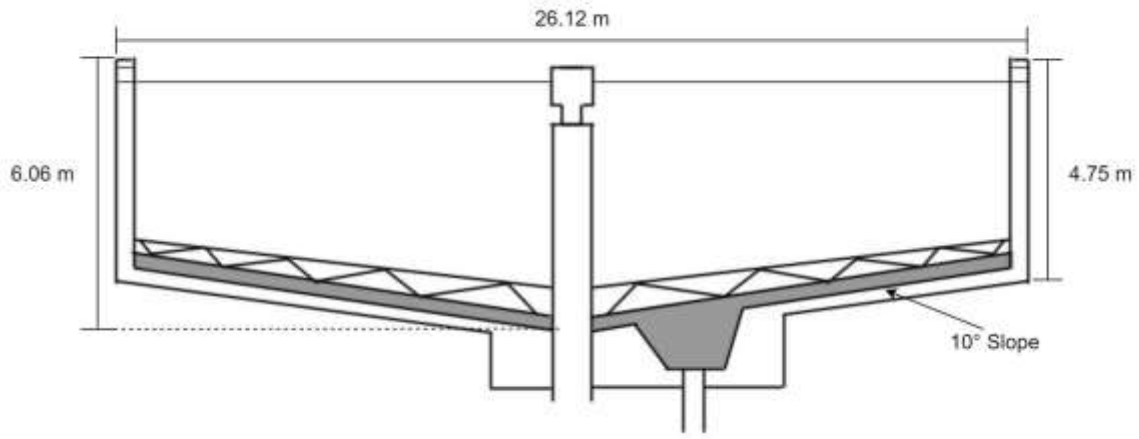

Figure 5.4.1 Dimensions of the circular sedimentation tanks.

As mentioned previously, the flow must be lower than 29.67 m/day to allow the maximum amount of suspended solids to settle out. Therefore, 24 $m^3/(day*m^2)$ was chosen as the surface overflow rate for the rectangular sedimentation tank. The circular tanks are used as a small pre-treatment to remove additional solids. Clarifiers with this purpose typically flow faster, with surface overflow rates of 24-32 $m^3/(day*m^2)$ (Scholz, 2015). To remain below the settling velocity of the finest anticipated particles, a surface overflow rate of 28 $m^3/(day*m^2)$ was chosen for the circular sedimentation tanks. Due to the variation in river quality and flow, the sedimentation tanks were designed with a maximum flow capacity of 15,000 m^3/day. This is 12.7% above the expected flow and ensures that the system can handle heavy precipitation events or instances of excessive contamination. All parameter values for both types of sedimentation tanks can be found in Table 5.4.1, below.

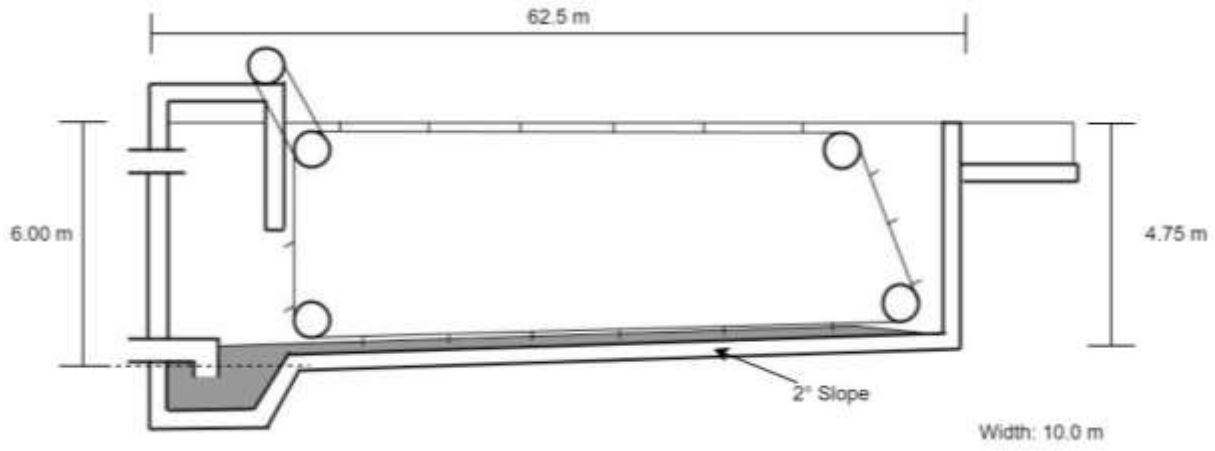

Figure 5.4.2 Dimensions of the rectangular sedimentation tank.

Using the chosen values for surface overflow rate and volumetric flow of each sedimentation tank, the individual surface areas were calculated using (5.4.1), below.

$$Surface\ overflow\ rate\ = \frac{Flow\ rate, m^3/day}{Surface\ Area, m^2} \tag{5.4.1}$$

For the circular and rectangular sedimentation tanks, the surface area was determined to be 535.71 m^2 and 625 m^2, respectively. The volume of each tank was then calculated by multiplying the depth of the tank and the surface area, and was used in (5.4.2) to determine the detention time.

$$Detention\ time, hr\ = \frac{Volume\ of\ tank, m^3}{Flow\ rate, m^3/day} * 24 \tag{5.4.2}$$

As expected, the circular sedimentation tanks have a slightly lower detention time due to the faster surface overflow rate. These tanks detain the water for an average of 3.43 hours, while the rectangular tank holds the water for an average of 4 hours.

As a precautionary measure, the scour velocity of the fine nylon fibers was calculated to determine if the flow of the sedimentation tank would move settled fibers back into the overflow. To determine the scour velocity, equation (5.4.3) - found in a paper detailing the design of sedimentation tanks in the Journal of Environmental Engineering - was used

$$V_{sc} = \frac{k*(s-1)gd_{sc}^2}{3\nu}\left(\frac{Q}{\nu B}\right)^{0.125} \tag{5.4.3}$$

where V_{sc} is the scour velocity, k is the ratio of shear velocity to fall velocity, s is the specific gravity, g is the gravitational constant, d_{sc} is the diameter of the particle, ν is the kinematic viscosity, Q is the flow rate, and B is the width of the tank (Swamee & Tyagi, 1996). The scour velocity was calculated to be 91.28 m/h, much greater than the surface overflow rate. This design, therefore, will not cause the sludge to be pulled back into the overflow.

Table 5.4.1 Defining parameters for both sedimentation tank designs.

Parameter	Circular Tank	Rectangular Tank
Scour Velocity (m/h)	91.28	91.28
Detention Period (hr)	3.43	4.00
Avg. Water Depth (m)	4.00	4.00
Volume of Basin (m^3)	2142.86	2500.00
Flow Rate (m^3/day)	15,000.00	15,000.00
Surface Overflow Rate (m^3/day/m^2)	28.00	24.00
Surface Area (m^2)	535.71	625.00
Weir Length (m)	82.01	75.00
Weir Overflow Rate (m^3/day/m)	182.91	200.00
TSS Removal Rate (%)	60.00	65.00

To calculate the estimated removal rate of TSS from the sedimentation tanks, the ratio of the surface overflow rate to water depth was calculated for each tank in [gal/(ft^2*day)]/ft. These values were compared to Figure 5.4.3, a graphical relationship between the aforementioned ratio and TSS removal created by the US Department of the Interior (Smith, 1967). Using the graph, the TSS removal is 60% for the circular tanks and 65% for the rectangular tank. This data aligns with the larger surface area and slower overflow rate of the rectangular tank. These values were used to determine the mass and volume balances displayed in Table 5.2.1.

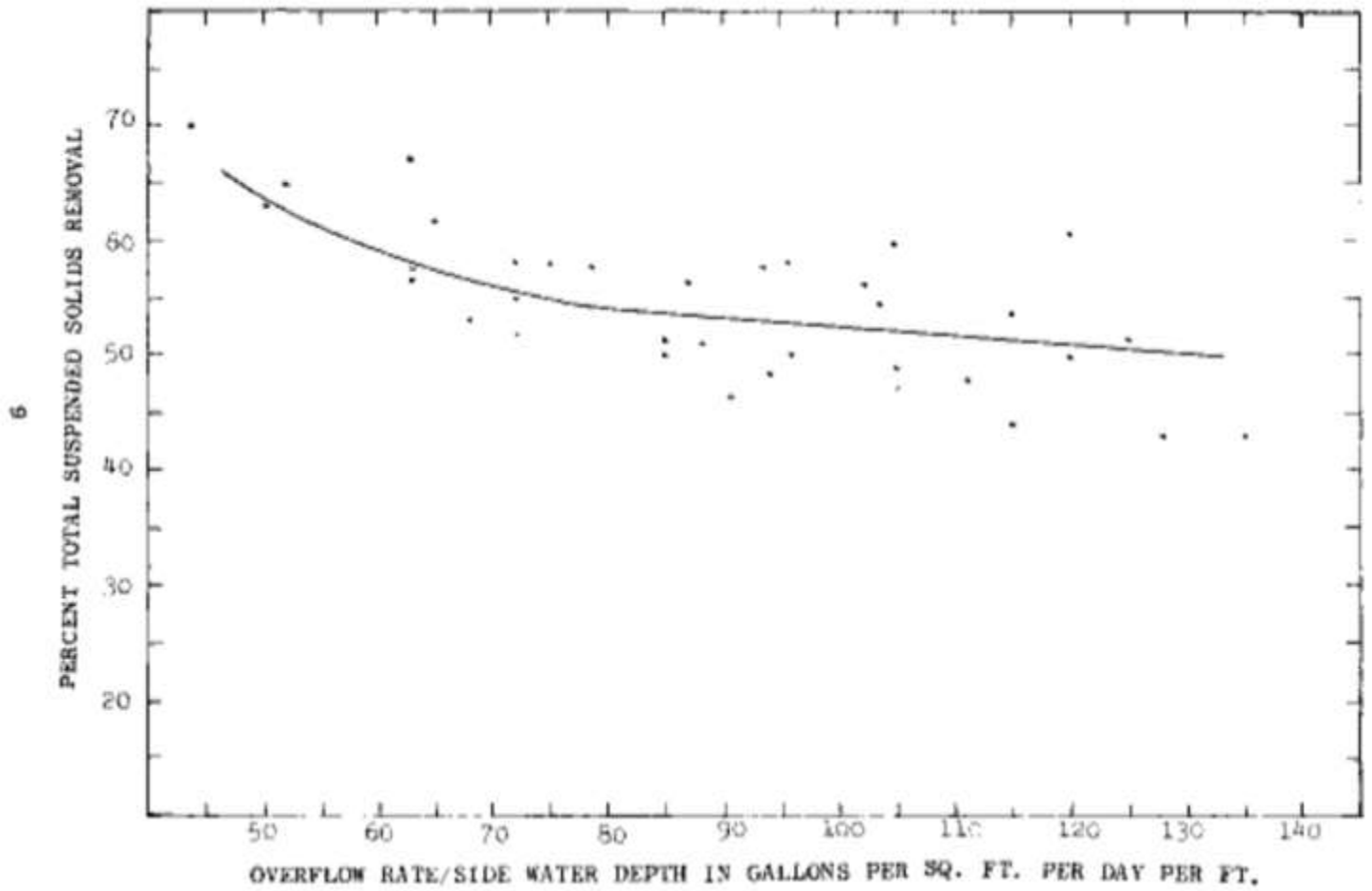

Figure 5.4.3 Graph of TSS removal and overflow rate to water depth ratio published by the US Department of the Interior. (Smith, 1967)

5.5 Pumping Power Requirement

The pumps in sedimentation must be able to effectively move the water from screening to sedimentation and from tank to tank. However, to avoid short-circuiting the sedimentation tanks, it is important to keep the flow at atmospheric pressure and low speed. Therefore, the entering and exiting pressure from pumps P-101 and P-102 (see Figure 5.1.3) is atmospheric. To calculate the total pressure drop for the pumps, frictional losses in the pipes and control valves must be considered. In all pumping calculations, it is assumed that frictional losses in pipes and control valves each add 0.50 atm (0.507 bar) to the total pressure drop. The formula used to determine the pressure drop in pump P-101 is below

$$\Delta P_{pump} = P_{tank} - P_{screening} + FL \tag{5.5.1}$$

where ΔP_{pump} is the pressure loss, P_{tank} is the pressure at the radial tank, $P_{screening}$ is the pressure at the bar screen, and FL is the total frictional losses. For pump P-101, ΔP_{pump} is 1.00 atm (1.01 bar). A calculation for pump P-102 led to an identical answer for pressure loss. Once these pressure drops were calculated, the power required to bring the water to the necessary pressure was determined using (5.5.2)

$$P = Q * \Delta P_{pump} \tag{5.5.2}$$

where Q is the total feed volumetric flow rate going into sedimentation (0.154 m^3/sec). As seen in Table 5.2.1, the volumetric flow rate decreases marginally between the circular tank and the rectangular tank. For the pumping calculations, it is assumed that the volumetric flow rate is the

same for both pumps. Assuming 75% efficiency, the total pumping power requirement for sedimentation 41.59 kW

5.6 Primary and Secondary Tank Cleaning

The cleaning for both the circular and rectangular sedimentation tanks is automated and uses mechanical sludge scraping systems. The circular tanks use rotational systems with multiple scraper arms to push the sludge into a through at the center of the tank. These arms move at a velocity of 0.02 rpm. This is slightly slower than the scour velocity of the fine nylon fibers, which is 0.03 rpm. Additionally, this scraper velocity aligns with standard industry values cited in literature (Scholz, 2015). The rectangular tank uses a chain-and-flight sludge collection system. A system of pulleys moves metal bars extending across the tank in a cyclical motion, as seen in Figure 5.1.2. As the bars reach the bottom of the tank, they scrape the sludge down the sloped floor, toward a collection trough near the inlet of the tank. The sludge scraper moves at 0.9 m/min, well below the scour velocity of 1.5 m/min. Again, this scraper velocity falls within typically cited ranges for industry standards (Scholz, 2015). In both tanks, the sludge is pumped from the collection trough and moved to a holding tank for HTL.

Because of the dilute nature of the river water, and the pre-screening before sedimentation, excessive buildup of sludge is not expected. In fact, very little sludge is actually collected through sedimentation, and most of the contaminants are removed further downstream. Because of this, there is no regular cleaning anticipated outside of the mechanical sludge collection systems.

6. Microfiltration

6.1 Introduction

Any suspended solids and microorganisms in the water that come out of the sedimentation pond will be sent to microfiltration for removal. These suspended solids can be measured using a parameter called Total Suspended Solids, herein referred to as TSS. TSS includes a variety of solid materials that can be distributed in the river water including silt, sand, decaying plant and animal matter, industrial wastes, pesticides, and metals (Murphy, 2007). When microorganisms like bacteria are removed from the water, the biological oxygen demand (BOD) and chemical oxygen demand (COD) concentrations will decrease as a result, and any microorganisms that manage to bypass the filter and reverse osmosis membranes will be killed with UV treatment. Both TSS and microorganisms can cause damage to the reverse osmosis membranes by clogging pores, so it is important to remove them with microfiltration as much as possible.

The microfiltration in this design will consist of Pall Water hollow fiber bundles with 0.1 µm size pores (Pall Water, 2022-b) encased inside 24 Pall Water Microza Hollow Fiber UNA Modules (Pall Water, 2022-a). Both of these can be seen in Figure 6.1.1. These hollow fiber bundles operate with an outside to inside flow configuration. This means that the water is fed on the outside of the hollow fibers, and the small pore sizes allow water to flow to the inside of the hollow fibers while keeping out any suspended solids and microorganisms (Pureflow Inc., 2018). A diagram of this configuration can be seen in Figure 6.1.2. The dirty water, concentrated with TSS and microorganisms, will be sent out of the module with a reject stream and sent to hydrothermal liquefaction where it will be further processed.

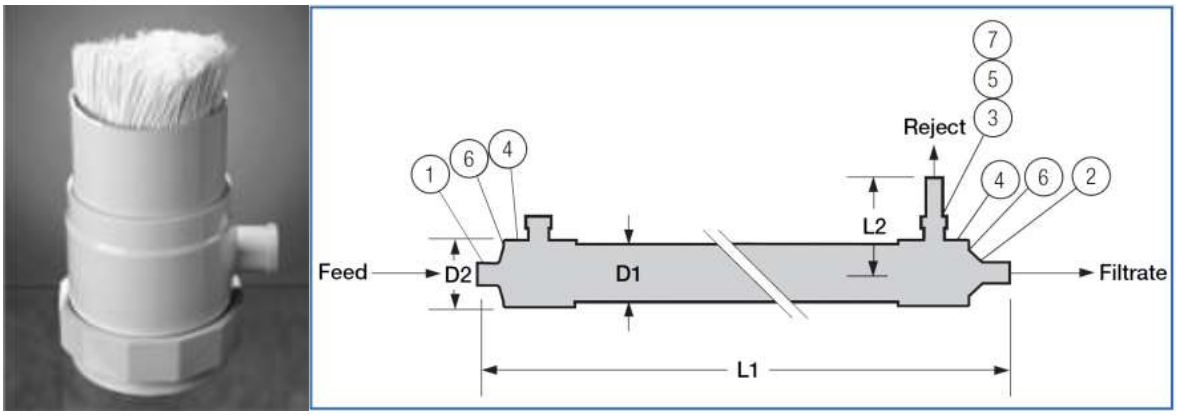

Figure 6.1.1 Hollow fibers inside of Microza UNA modules cutaway (left), and diagram of Microza UNA modules (right). (Pall Water, 2022-a)

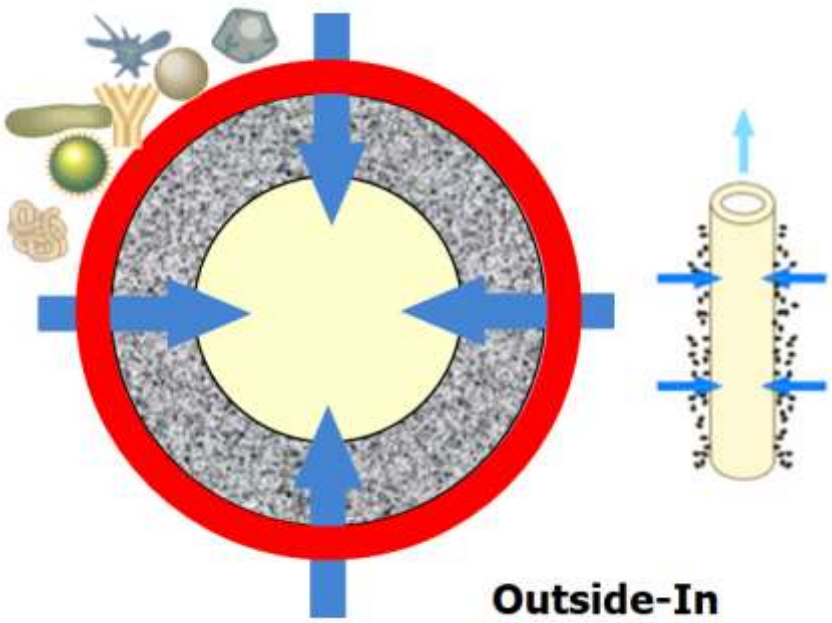

Figure 6.1.2 Outside to inside filtration configuration diagram. (Pureflow Inc., 2018)

6.2 Design and Material Balances

Based on the water flux of 440 $Lm^{-2}hr^{-1}$ and the membrane area of 50 m^2 given from the manufacturer (Pall Water, 2022-b), it was determined that 24 hollow fiber microfilter modules would be needed to achieve the desired permeate flux of 12,672 m^3/day. The flow rate to the entire microfiltration process was determined to be 13,304.50 m^3/day. This number was

determined to be the sum of the aqueous co-product flow rate (see section 9.1) from HTL (6.73 m^3/day) and the average overflow rate for both seasons from sedimentation of 13,297.77 m^3/day.

With the number of modules determined, material balances were performed based on several assumptions. Firstly, it was assumed that the microfilters would remove all TSS from the water, resulting in permeate water containing 0 mg/L of TSS. This is a fair assumption due to the low concentration of TSS in the feed and the large size of the particles in the river. Suspended sediments in the Cooum River, for example, range in size from 75 to 425 μm (Abinandan et al., 2019). Secondly, the removal percentage of BOD and COD was assumed to be the same as that used in a previous capstone thesis (Kohl et al., 2019). This means that the mass of BOD would be reduced by 93.25% and the mass of COD would be reduced by 93.38%. Since the designers of this previous thesis used the same outside to inside hollow fiber bundle configuration and because another study confirms that a similar reduction of 91% of BOD and COD can be obtained (Bhattacharya et al., 2013), this is a fair assumption. Lastly, it was assumed that the water recovery in the permeate would fall in the range of 95-98%, according to the manufacturer's data sheet (Pall Water, 2022-a).

With these assumptions in mind, the feed flow rate per microfilter unit was calculated by dividing the feed flow into microfiltration by the 24 modules needed for the process. This gives a feed flow rate per microfilter of 554.35 m^3/day. Based on a water flux of 528 m^3/day per filter module, it was determined that the water recovery in the permeate would be 95.25%, which falls in the range stated by the manufacturer. This leaves a retentate flow rate per unit of 26.35 m^3/day, which will be sent to HTL. Adding this all together for 24 microfilter units, the flow rates can be seen in Figure 6.2.1. Two material balances were performed for microfiltration, one for the pre-monsoon season and one for the post-monsoon season (as the concentrations of TSS,

BOD and COD vary significantly between the two seasons). Using the assumed reductions of BOD and COD from the previous thesis (Kohl et al., 2019), the concentrations of BOD, COD and TSS for each stream can be seen in Table 6.2.1.

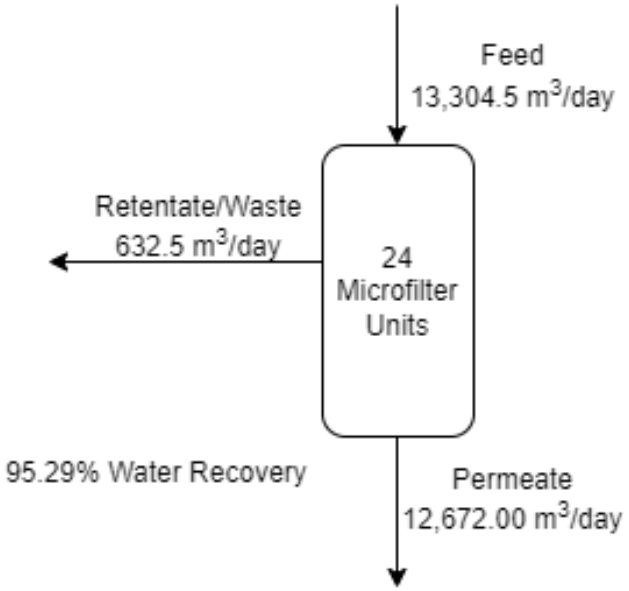

Figure 6.2.1 Microfiltration flow rates.

Table 6.2.1 Microfiltration mass balances for both seasons.

Pre-monsoon Balances			Post-monsoon Balances		
Stream	Substance	Conc. (mg/L)	Stream	Substance	Conc. (mg/L)
Feed	BOD	14.70	Feed	BOD	20.70
	COD	114.70		COD	52.90
	TSS	49.30		TSS	22.75
Permeate	BOD	1.04	Permeate	BOD	1.47
	COD	7.98		COD	3.68
	TSS	0.00		TSS	0.00
Retentate	BOD	288.32	Retentate	BOD	406.01
	COD	2252.91		COD	1039.05
	TSS	1037.01		TSS	478.54

6.3 Pressure Drop and Pumping Power Requirement

To determine the pressure drop across the hollow fiber bundle modules, a permeate pressure must be estimated. It is worth noting that all pressures reported from now on are gauge pressure unless they are stated to be atmospheric pressures. There are a few factors that must be considered when estimating permeate pressure. First, excessively high pressures on the microfilter cost more money to implement and may cause damage to the filters, so the permeate pressure should be close to atmospheric. Second, little driving force is needed to push permeate water to the next stage, as a pump pressurizes the water before it enters reverse osmosis. Taking into account these factors, a permeate pressure of 2 bar was chosen for each microfiltration module.

The applied pressure for microfiltration that is applied both to the feed and the retentate is the driving force for microfiltration. Pressure drop along the membrane was neglected, meaning that the feed and retentate operating pressures were approximated as the same value. Equation (6.3.1) was used to determine the applied pressure on the membrane.

$$Q = K * \Delta P * A \tag{6.3.1}$$

where K is the hydraulic permeability constant of the hollow fiber bundles, ΔP is the pressure drop between feed and the permeate, A is the active filtration surface area, and Q is the volumetric permeate flow rate per filter. The hollow fibers that are used are made of polyvinylidene fluoride (PVDF), which has a hydraulic permeability constant of $37.9*10^{-9}$ $m^3/(m^2*s*Pa)$ taken from a study focusing on hollow fibers of this same material (Darestani et al., 2014). This results in a ΔP value of approximately 0.03 bar.

Once this pressure drop was calculated, the pumping power required to bring the pressure of the water up to the appropriate value was determined using Equation (5.5.2) above, where Q is the total feed volumetric flow rate going into microfiltration (13,304.50 m^3/day) and ΔP_{pump} is the pumping pressure required to push the water through the membrane while overcoming any frictional losses in pipes (assumed to be 0.5 atm or 0.506625 bar) and in centrifugal pump valves (also assumed to be 0.506625 bar). This extra additional pressure should be enough to push water through the membranes and make up for the low value of ΔP. The pumping pressure required to drive the water into the microfiltration units was determined with (6.3.3),

$$\Delta P_{pump} = P_0 - P_{-1} + FL \tag{6.3.3}$$

where P_0 is the operating pressure of the feed water going into the microfiltration units, P_{-1} is the operating pressure of the water flowing into the pump, and FL is the frictional losses that must be overcome. With pressure drop and permeate pressure determined and the assumption that the applied pressure along the membrane is constant, the feed and retentate pressures of microfiltration were determined. The pumping power requirement for microfiltration was then determined to be 62.53 kW (assuming 75% efficiency).

6.4 Microfiltration Cleaning

Our system runs continuously, replacing microfiltration and reverse osmosis membranes when needed to prevent plugging, loss of flux, and loss of salt rejection (Puretec, n.d.-b). In order to maintain a consistent flux and salt rejection between membrane replacements, the membranes are backflushed with permeate water throughout the day. Backflushing, if done correctly, allows

the membranes to operate with lower chances of plugging and fouling of the membrane (Basu, 2014).

Throughout normal operation, one microfilter unit from each stage will be backflushed with a portion of the permeate stream equal to the flux one microfilter produces in the microfiltration process. One microfilter unit will take a total of three minutes to be backflushed completely, then automatically switched back into operation. The next microfilter unit will then be automatically switched off and backflushed in a similar fashion. For 24 microfilter units, an entire backflushing cycle will take approximately 72 minutes to complete and will be continuously cycling throughout the units during normal operating procedures.

To further ensure that the membranes are operating at high flux without fouling or plugging, they will be chemically cleaned once every three months (AWC, n.d.). Because the dissolved solids in the water consist of inorganic salts, metal oxides, and silt-like particles, the membranes will be cleaned with 1.0% (W) sodium dithionite ($Na_2S_2O_4$) at 25^oC and pH 5, which is able to handle removing each of these foulants (DuPont, 2022). Similar to backflushing, chemical cleaning will occur along with normal operation. One microfilter unit will be chemically cleaned while the others produce clean water. The cleaning process for one microfilter unit will take approximately two hours: one hour to soak the membranes with the cleaning solution and another hour to run the cleaning solution through the pressure vessel. The cleaning process will take approximately two days to complete for microfiltration.

The cleaning solution flow rate depends on how many microfilter units are in the microfiltration system. The cleaning solution flow rate for microfiltration is 3,600 m^3/day (DuPont, 2022). As seen in Figure 6.4.1, below, the cleaning solution flows from a 10,000 m^3 tank into each microfilter unit and reverse osmosis stage. The solution flows through the

membranes and is recycled back into the tank where it will be drained once the cleaning process is complete.

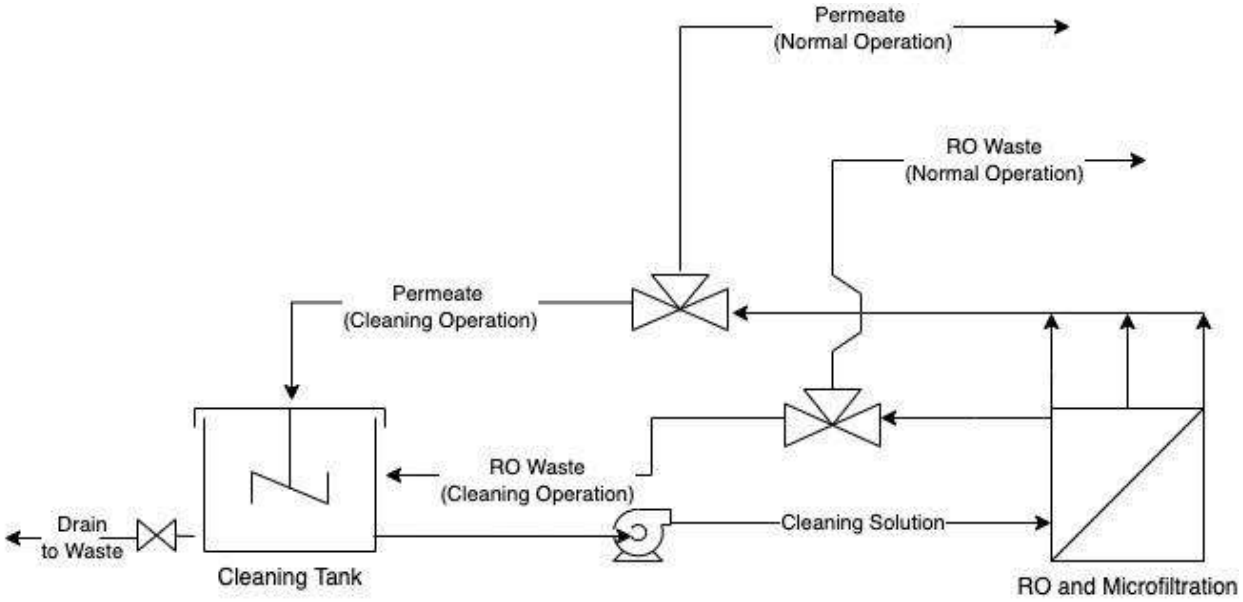

Figure 6.4.1 Process flow diagram of the chemical cleaning system.

7. Reverse Osmosis

7.1 Introduction

Water that comes out of microfiltration will be sent to the reverse osmosis units to remove dissolved solids (quantified as Total Dissolved Solids, TDS) from the water. TDS encompasses dissolved minerals, metals, organic material, and salts (Corrosionpedia, 2019). This process makes use of spiral wound membranes from Dupont's Filmtec catalog. These membranes work by feeding dirty water on the outside of the central permeate flow tube. Membranes wrapped around the permeate flow tube allow clean water to flow through under sufficient pressure while keeping out dissolved solids. Dirty water is retained on the outside of the permeate flow tube. An illustration of a spiral wound setup can be seen in Figure 7.1.1. These membranes are designed to remove any remaining particles with a diameter greater than 0.001 μm (Hancock, 2018). This process is the last step in removing unwanted solid particles in the water, before UV treatment kills all remaining microorganisms.

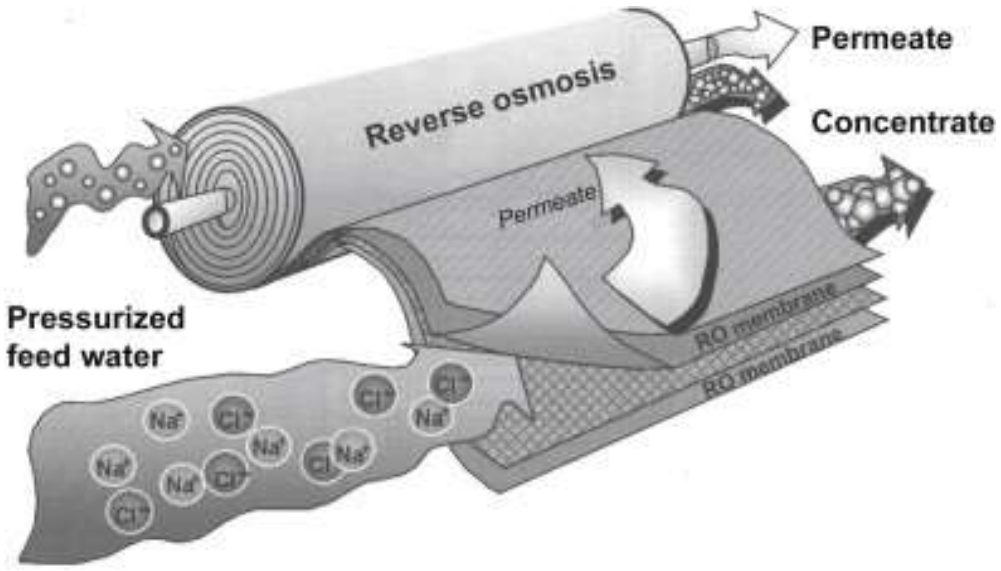

Figure 7.1.1 Spiral wound reverse osmosis membrane setup. (Daal et al., 2015)

7.2 Design and Material Balances

In designing the RO system, spiral wound membranes are placed inside vessels to which high pressure is applied. There are typically between six to eight spiral wound membrane units in one pressure vessel (ScienceDirect, 2015). Pressure vessels are arranged in parallel to form stages, so as to divide the feed evenly for faster processing. Pressure vessels are placed under applied pressures that are greater than their osmotic pressures to drive RO. Stages are placed in series to allow as much permeate to be obtained from the river water as possible. Each stage is placed under a different applied pressure depending on the stage's osmotic pressure. The ion concentrate from a stage becomes the feed for the next stage to recover additional water.

Increasing the number of stages leads to greater water recovery, but this means that the feed to the next stage becomes more and more concentrated with TDS. This can cause damage to the membranes when solubility limits are exceeded, and as the number of stages increase the little water that is recovered in the permeate may not worth the membrane damage (Fravel, 2014). With this and the desired permeate recovery goal in mind, a three stage RO system was designed. The number of pressure vessels decreases as the stage number increases because the water flow rate decreases per stage, requiring less membrane surface area.

Two material balances were performed for RO, one for the pre-monsoon season and one for the post-monsoon season. The feed concentration going into the first stage was taken as the average TDS concentrations over the past three years for both pre and post-monsoon seasons (Chennai Rivers Restoration Trust, 2020). The mass concentration of TDS in the river water is high in the pre-monsoon season, inducing large osmotic pressures and therefore requiring high applied pressures to drive RO. As a result of rain dilution, the TDS concentration is much lower in the post-monsoon season, leading to lower osmotic and applied pressures. In choosing the

types of membranes that were needed, it was important to quantify the purity of water that is in the river feed. Brackish water has a TDS concentration less than or equal to 10,000 mg/L, while seawater has a TDS concentration greater than 10,000 mg/L (Godsey, n.d.). While the river feed can be classified as brackish water year-round, material balances for the first stage in the pre-monsoon season (Figure 7.2.1) determined that the concentration of the ion waste coming out of the first stage classified it as seawater. Therefore, it was determined that the first stage would be composed of Dupont brackish water membranes with a permeate flux of 40 m^3/day and a salt rejection of 99% (2020b). Due to the ion concentrate of stage one meeting qualifications for seawater, the second and third stages would be composed of Dupont seawater membranes with a permeate flux of 28 m^3/day and a salt rejection of 99.8% (2020).

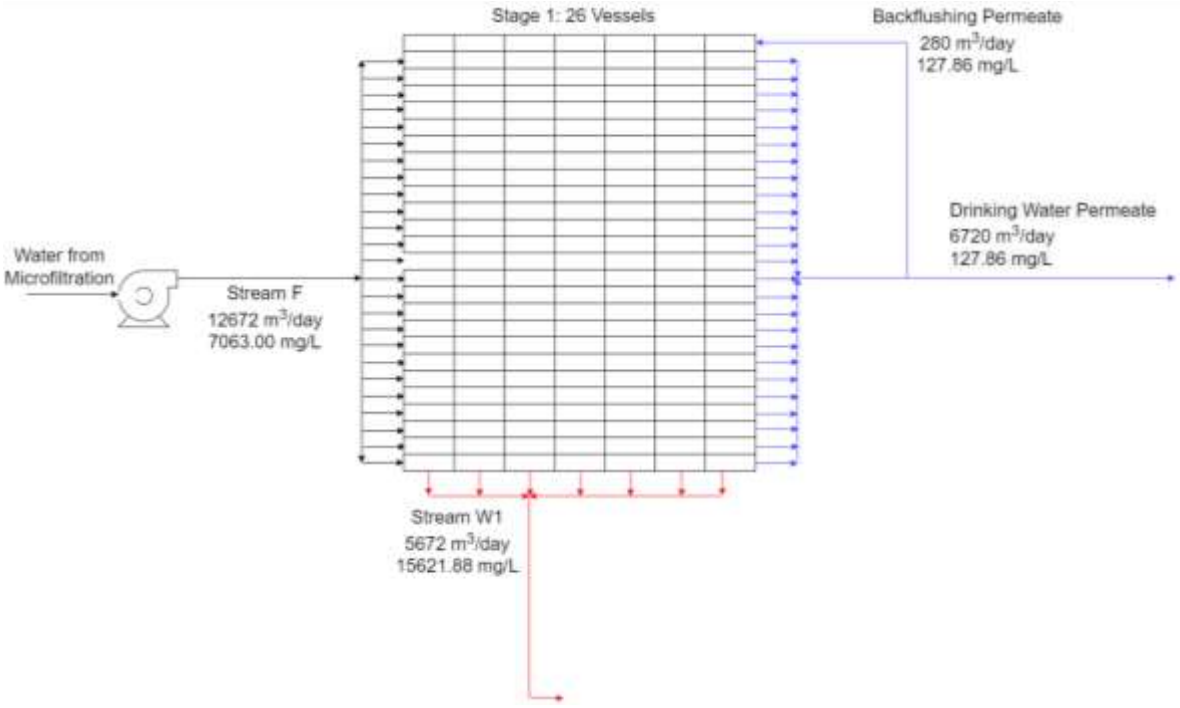

Figure 7.2.1 Material balance for stage one (pre-monsoon season).

The entire RO arrangement, including pumps, valves, and pressure vessels, can be seen in Figure 7.2.2. Material balances for the process can be seen in Table 7.2.1. In determining the

number of pressure vessels needed for the entire process, the permeate flow base value was started at 10,000 m^3/day. Equation (7.2.1) was used to determine how many vessels were needed.

$$10{,}000\ m^3/day = d(40a + 28b + 28c) \quad (7.2.1)$$

where a is the number of pressure vessels in stage one, b is the number of pressure vessels in stage two, c is the number of pressure vessels in stage three, and d is the number of membranes in each vessel. Initially, it was estimated that a = 2b and b = 2c, and it was assumed that a = 24, b = 12, and c = 6. Assuming that each vessel contains 7 membranes (d = 7) gives the following:

$$7*(40*24 + 28*12 + 28*6) = 10{,}248\ m^3/day.$$

This exceeds the target permeate flux, so one vessel was subtracted from stage three to give 5 main pressure vessels in stage three. One extra vessel was then added to each stage to collect backflushing water, and another extra vessel was added to each stage to allow for the cleaning of one vessel at all times without reducing productivity (see section 7.6). Accordingly, stage one consists of 26 pressure vessels, stage two consists of 14 pressure vessels, and stage three consists of 7 pressure vessels. This gives a total backflushing flow rate of 672 m^3/day while the permeate flux is 10,052 m^3/day.

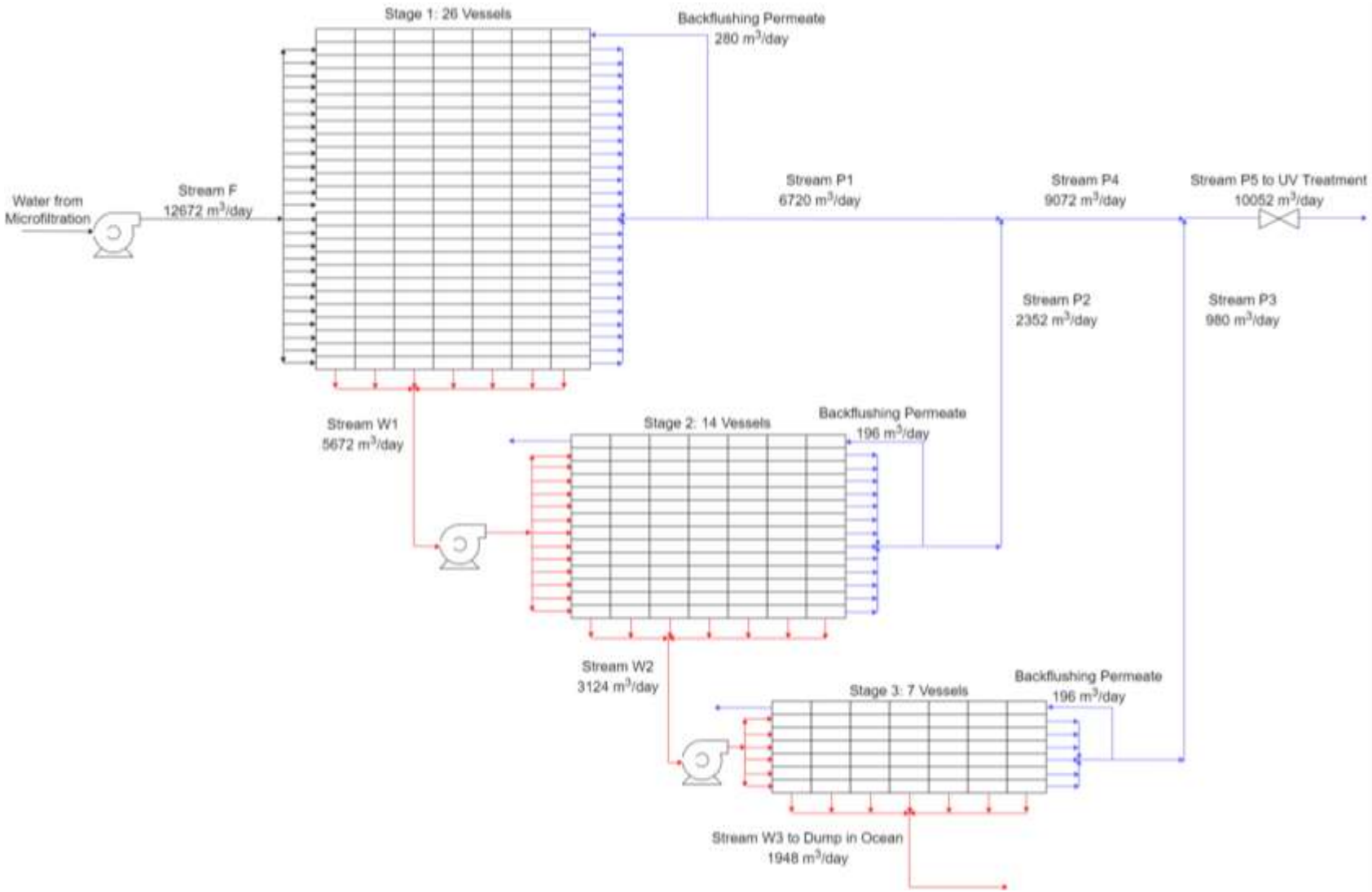

Figure 7.2.2 Arrangement of pressure vessels and flow rates by stage.

Table 7.2.1 Material balances for pre-monsoon and post-monsoon seasons.

Stream	Pre-monsoon Season	Post-monsoon Season
	Concentration of TDS (mg/L)	Concentration of TDS (mg/L)
F	7063.00	1326.00
W1	15621.88	2932.84
W2	28306.69	5314.27
W3	45304.54	8505.42
P1	127.86	24.00
P2	69.55	13.06
P3	150.39	28.23
P4	112.30	21.08
P5	116.48	21.87

7.3 Osmotic Pressures

The osmotic pressure was calculated using Equation (7.3.1).

$$\Pi = R * T * Cs * i * \Phi \tag{7.3.1}$$

where R is the universal gas constant (8.314 $\frac{m^3 * Pa}{mol * K}$), T is the absolute temperature (K), Cs is the molar concentration of total dissolved solids ($\frac{mol}{m^3}$), i is the number of ions that dissociates in solution (the Van't Hoff factor), and Φ is the osmotic coefficient of the solution. The molar concentration of TDS was determined by assuming that it primarily consists of NaCl, which is confirmed in a 2009 study by Giridharan et al. The molar mass of NaCl (58.44 g/mol), its osmotic coefficient (0.93), and its Van't Hoff factor (approximately 2) were used in calculating the osmotic pressure for both the feed and the retentate of each stage (Feher, 2017). These osmotic pressures can be seen in Table 7.3.1.

Table 7.3.1 Osmotic pressures of water at various points in the process.

Stage	Pre-monsoon Season Pressures (bar)		Post-monsoon Season Pressures (bar)	
	Feed Osmotic Pressure	Retentate Osmotic Pressure	Feed Osmotic Pressure	Retentate Osmotic Pressure
1	5.59	12.37	1.05	2.32
2	12.37	22.41	2.32	4.21
3	22.41	35.86	4.21	6.74

7.4 Applied and Permeate Pressures

The appropriate applied pressure was determined for each stage to ensure that enough driving force can push river water through the membranes and drive permeate water toward UV disinfection. Applied pressure (AP) was determined with equation (7.4.1),

$$AP = P_{permeate} + TMP \tag{7.4.1}$$

where $P_{permeate}$ is the operating pressure of the permeate (bar) leaving the stage and TMP is the transmembrane pressure required to push water through membranes. A pressure of 2 bar was determined to be sufficient as the permeate pressure for all stages during both seasons.

Transmembrane pressure (TMP) is defined as the average of feed and ion waste operating pressures minus the permeate operating pressure (Twiford, 2022), which can be seen in (7.4.2).

$$TMP = \frac{P_{feed}+P_{ion\ waste}}{2} - P_{permeate} \tag{7.4.2}$$

Since the operating pressures of the feed and ion waste cannot be determined directly, (7.4.3) will be used as a basis to determine transmembrane pressure,

$$\mu_p = K(\triangle P - \Delta\Pi) \tag{7.4.3}$$

where μ_p is the linear permeate velocity (m/sec), ΔP is the difference between feed and permeate operating pressures (bar), $\Delta\Pi$ is the difference between feed and permeate osmotic pressures, and K is the hydraulic water permeability constant. The permeate osmotic pressure was approximated as zero due to its very low TDS concentration in each stage. K depends on the membrane used in the process, and the constant for brackish water membranes was obtained directly from literature as 0.11 gfd/psi ($2.78*10^{-5}$ m/(sec*bar)) (Li, 2012). The K constant for

seawater membranes was estimated as the average of constants of two membrane models, SW30XLE-400 and SW30HR-380 (Lu et al., 2007), which results in a value of $1.15*10^{-5}$ m/(sec*bar). The permeate flux could be estimated by taking the membrane volumetric flow rate given by the manufacturers and dividing that value by the active membrane surface area (37 m^2 for both membranes). With (7.4.3) in mind, the TMP can be determined with (7.4.4),

$$\mu_p = K(TMP - \Pi_{avg}) \tag{7.4.4}$$

where Π_{avg} is the average of the feed and ion waste osmotic pressures (bar).

Once transmembrane pressures were obtained, applied pressures for each stage could be calculated. The results for applied pressure can be seen in Table 7.4.1. The frictional losses along the membranes was neglected in the calculations of applied pressure. Because of this, the applied pressure that is calculated is the same for both the feed and retentate applied pressures. To verify the validity of this assumption, typical applied pressures for brackish and seawater were researched and compared to the calculated values. According to the Texas Water Development Board (n.d.), the applied pressure for membranes handling seawater (with a feed concentration of greater than 35,000 mg/L TDS) is typically in the range of 50-80 bar. Brackish water typically requires applied pressures that are significantly lower in the range of 10 to 25 bar (Semiat, 2010). As stage three during the pre-monsoon season is the only stage that comes close to this high of a feed concentration, it makes sense that this is the only stage requiring an applied pressure above 50 bar. The applied pressure of stage two for the pre-monsoon season is 47.63 bar, which is expected as the TDS feed concentration is much greater than that of brackish water but less than that of seawater.

Table 7.4.1 Applied and permeate pressures for reverse osmosis.

Pre-monsoon Season			Post-monsoon Season		
Stage	Type of Water	AP (bar)	Stage	Type of Water	AP (bar)
1	Brackish	27.61	1	Brackish	20.32
2	Seawater	47.63	2	Brackish	33.51
3	Seawater	59.38	3	Brackish	35.72

7.5 Pumping Power, Energy Requirements

Determining the power required to pump water through the membranes was very similar to the same process used to determine the required pumping power for microfiltration, so equation (6.3.2) was used to estimate this. In this case, Q is the volumetric flow rate of feed water going into a stage (m^3/sec) and $\Delta Ppump$ is the pumping pressure required to push the water through the membrane while overcoming any frictional losses in pipes or centrifugal pump valves (both assumed to add 0.5 bar). The pumping pressure required to drive the water into the membranes in a particular stage was determined with (6.3.3), where P_0 is the operating pressure of the feed water going into the stage, P_{-1} is the operating pressure of the water flowing into the pump, and FL is the frictional losses. The feed and retentate pressures of each stage are determined using the calculated applied pressure and the assumption that this applied pressure is constant along the membrane. The results for pumping power requirements can be seen in Table 7.5.1. Since the permeate is collected at 2 bar and does not need to enter UV treatment at any specific pressure, a valve should be sufficient to control the flow of permeate to UV treatment.

Table 7.5.1 Pumping power requirements for RO.

Stage	Pre-monsoon Season Power Values (kW)	Post-monsoon Season Power Values (kW)
1	520.64	378.04
2	184.13	124.36
3	61.52	15.52
Total	766.29	517.92

7.6 Membrane Cleaning

The cleaning procedures for microfiltration and RO are the same. Throughout normal operation, one pressure vessel from each stage will be backflushed with a portion of the permeate stream equal to the flux one vessel produces in the reverse osmosis process. One pressure vessel will take a total of three minutes to be backflushed completely, then automatically switched back into operation. The next pressure vessel in the stage will then be automatically switched off and backflushed in a similar fashion. Pressure vessels in different stages will be cleaned simultaneously. An entire backflushing cycle will take approximately 30 to 90 minutes to complete, depending on the stage, and will be continuously cycling throughout the stage during normal operation procedures.

Similar to microfiltration, the RO membranes will be chemically cleaned with a 1.0% (W) sodium dithionite solution to maintain a high flux without fouling or plugging. The cleaning process for each pressure vessel will take approximately two hours: one hour to soak the membranes with the cleaning solution and another hour to run the cleaning solution through the pressure vessel. The cleaning process will take approximately two days to complete for stage one, one day to complete for stage two, and half a day to complete for stage three.

The cleaning solution flow rate changes for each stage, depending on how many pressure vessels are in the stage. The cleaning solution flow rate for stage one, two, and three are 3,600 m^3/day, 1,900 m^3/day, and 900 m^3/day respectively (DuPont, 2022). As seen in Figure 6.4.1, the cleaning solution flows from a 10,000 m^3 tank into each RO stage. The solution flows through the membranes and is recycled back into the tank where it will be drained once the cleaning process is complete.

7.7 Ion Waste Disposal

Throughout the filtration process, the inlet river water is purified via the removal of contaminants from the water. Reverse osmosis has a clean permeate stream and a concentrated waste stream. The reverse osmosis waste stream flows at a rate of 2,448 m^3/day with a TDS concentration of about 49,020 mg/L and 9,200 mg/L during pre-monsoon and post-monsoon seasons respectively.

India has several regulations regarding industrial waste management and disposal methods. One such regulation is the Water Prevention and Control of Pollution Cess Act of 2003 (Furtado, 2021). This act along with previous regulations defines industrial waste and states that any disposal or dumping of industrial effluent into Indian rivers would incur a tax. The waste from reverse osmosis in this plant falls into this Act's definition of industrial waste and would result in our having to pay a tax. In order to avoid this tax, waste will be pumped directly to the nearest ocean, the Bay of Bengal. India currently has no regulations regarding disposal of waste into the ocean, thus the plant would not need to pay a tax on our waste disposal. Due to the

design location near the Napier Bridge at the mouth of the Cooum River, pumping waste into the Bay of Bengal would be easy and inexpensive.

The environmental impact of the waste on the Bay of Bengal would be insignificant. The Bay of Bengal has an average TDS concentration of 27,140 mg/L (Rashid et al., 2013). The waste concentration from the process is at an average of 29,110 mg/L. Due to the similarity in concentrations, the waste stream will not have an environmental impact on the quality of water in the Bay of Bengal.

8. Ultraviolet Disinfection

8.1 Introduction

At this point in the process, sedimentation and microfiltration have removed the settleable and suspended solids, and RO has removed pesticides, heavy metals, pharmaceuticals, and other chemical contaminants. However, human pathogens, including bacteria, viruses, and protozoa, remain in the water. A method for disinfection must be used to produce clean, potable water suitable for sale. The three most widely used methods for drinking water disinfection are chlorination, UV radiation and ozonation.

In municipalities with functional water pipelines, chlorination is typically favored. This method is very effective at inactivating pathogenic microorganisms and leaves a small amount of residual chlorine in the water. These residuals allow for protection against pathogens as the water moves through the pipelines (A. Mills, personal communication, February 15, 2022). The final product will be bottled, so these residuals are not necessary with sanitary bottling. Chlorination also produces many disinfection byproducts. The byproducts, including halogenated trihalomethanes and haloacetic acids, are carcinogenic and toxic (Gopal et al., 2007). Therefore, additional steps are needed to remove these contaminants, including adsorption or coagulation (A. Mills, personal communication, February 15, 2022). To avoid this additional cost and eliminate the risk of carcinogens in the water, chlorination was not chosen for the final disinfection.

Ozonation and UV disinfection do not result in disinfection byproducts. Ozonation presents many challenges, especially in India. The overall electricity and capital is very high, because ozone, an unstable gas, has to be generated on site (Central Pollution Control Board,

Ministry of Environment and Forests, n.d.). Additionally, maintaining a long enough contact time between the dissolved ozone and water is difficult in turbulent flows. Finally, high temperatures and humidity complicate ozone generation (Central Pollution Control Board, Ministry of Environment and Forests, n.d.). Chennai, being close to the ocean and the equator, is both humid and hot year round. UV disinfection does not require gases or mixing, and does not vary according to external conditions. For these reasons, UV disinfection was chosen for the water treatment plant.

UV disinfection systems use one or more UV lamps that produce UV-C rays in the germicidal spectrum. The frequency used in destroying microorganisms is 254 nm (ESP Water Products, n.d.). As seen in Figure 8.1.1, water in a UV disinfection system passes through a chamber containing the UV lamps. In the chamber, the pathogens are exposed to the UV light, and the DNA of the microorganisms is altered. This inhibits the pathogen's ability to function and eliminates further reproduction. This inability to replicate means that the microorganism can no longer infect a host, stopping the spread of any potential waterborne illnesses. UV disinfection destroys 99.9% of bacteria, viruses, and protozoa when adequate exposure time and lamp intensity is used (ESP Water Products, n.d.).

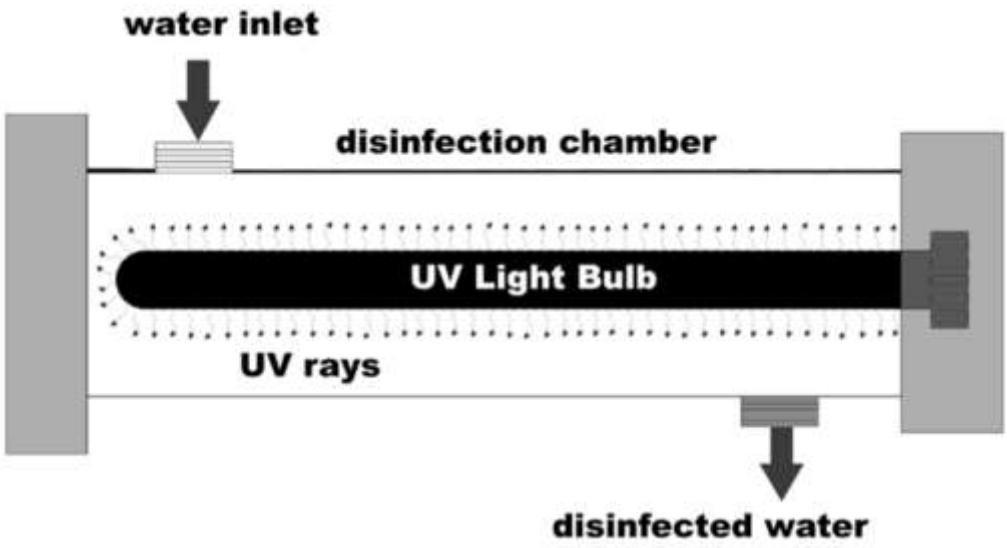

Figure 8.1.1 UV disinfection chamber with a single UV lamp. (Vitasalus, 2021)

8.2 Design and Material Balances

The microorganisms are not removed during the disinfection process, and no chemicals are added, so there is no change in mass, volume, or composition. Industrial UV disinfection units range in size. The largest unit that is readily available has a maximum flow capacity of 12,024 m^3/day. The system is listed as model "SUV-2206" by PureAqua, under their Industrial UV Sterilizer line (Bullard & Salas, n.d.). This unit would easily be able to handle the typical flow from the RO units, which is 10,052 m^3/day. Additionally, preliminary energy calculations revealed that one larger unit needs less power than two smaller units. Moreover, the maximum capacity of the unit is 17% above the flow in the facility. Operating well below the flow capacity allows for longer exposure time within the chamber. This increases the effectiveness of the disinfection process (ESP Water Products, n.d.). A visual of a UV system produced by PureAqua can be seen in Figure 8.2.1, below.

Figure 8.2.1 View of a small UV sterilization unit and its accompanying control panel. (Bullard & Salas, n.d.)

The chamber, constructed in 316L stainless steel, is 16” (41 cm) in diameter and accommodates UV lamps that are 60” (153 cm) long. The unit requires 12 UV lamps for operation. The maximum operating pressure is 10 bar and the range for operating temperature is 5-40°C (Bullard & Salas, n.d.). If the project were to move forward, the best solution would most likely be to work directly with PureAqua and utilize the option of purchasing a custom system.

8.3 Pumping Power, Energy Requirements

Due to the permeate exiting the RO units at 2 bar, a pump is not necessary to move the water into the UV chamber. The power requirement for the UV disinfection system is 2008 W, and the unit is operable 24 hours a day. Therefore, the daily energy expenditure of the system is $1.8*10^5$ kJ. After the water exits the UV chamber, it flows into cleaning containers for transportation to a bottling facility.

8.4 Cleaning and Waste Disposal

At the time of disinfection, the water has already been cleaned using multiple methods. As such, there is no threat of excessive buildup. Therefore, cleaning will take place annually, when the UV lamps are being replaced. During this time, the quartz sleeves will be removed and carefully inspected for damage. To protect workers from any potential hazards when performing maintenance on the unit, gloves and UV safety glasses will be worn (Outback Water, n.d.). If there is damage, the sleeve will be replaced. If not, a soft rag saturated with CLR will be used to clean the sleeve in order to prevent a film layer. Any buildup will diminish the UV transmittance and greatly decrease the effectiveness of the treatment. Every three years, all of the quartz sleeves will be replaced, even if there is no damage. This cleaning and replacement schedule follows manufacturer recommendations (Outback Water, n.d.). The old UV lamps and damaged sleeves cannot be disposed of in the landfill. The mercury content in the lamps presents health and environmental hazards if the glass is broken. Therefore, a local commercial disposal service will be contracted to properly transport and dispose of the discarded material.

9. Hydrothermal Liquefaction

9.1 Introduction

In recent advancements of biological waste treatment, hydrothermal liquefaction (HTL) has proven to be very effective on a lab scale. HTL describes the thermochemical depolymerization of biomass into liquid fuels where both subcritical or supercritical water is present at moderate temperatures and high pressures (Gollakota et al., 2018). The main reactions occurring at these conditions are ionic and free-radical reactions. These reactions break down the biopolymeric structure of solid organics to bio-crude oil (Gollakota et al., 2018). Additional products of this reaction are the aqueous co-product (ACP), char, and a mixture of gases. Due to the high water density of wet feedstock, the ACP usually holds a larger yield than that of the bio-crude oil. This has put large limitations on large scale HTL projects in the past. At the conditions required for HTL, water reaches its critical point, which changes its density, viscosity, and dielectric constants significantly (Elliott et al, 2015). The components within the reactor in these conditions form a supercritical mixture, making separations difficult.

The energy dense products from the HTL reactor will be used to power parts of the plant that are largely energy intensive. The reverse osmosis operation is one of these parts, requiring large quantities of energy to overcome osmotic pressure for the filtration of ~13,298 m^3/day of water. The HTL process will also be using sewage and organics from the Cooum River. The motivation for this is to clean the polluted river while also using that waste to generate electricity. The pollution in the river, mainly wet organic matter, is separated out in sedimentation tanks and fed into the HTL reactor. Wet organics like sewage sludge are ideal inputs for HTL because of their high moisture content (Snowden-Swan et al., 2016).

The HTL reactor is run by feeding steam to the reactor. This acts as a way to both heat the reactor and add moisture content to the water content dependent reaction. Once the reaction is completed, the contents are separated and combusted using a boiler that spins a turbine to generate electricity for the reverse osmosis and filtration sections of the plant. The design for the HTL section of the plant can be seen in Figure 9.1.1.

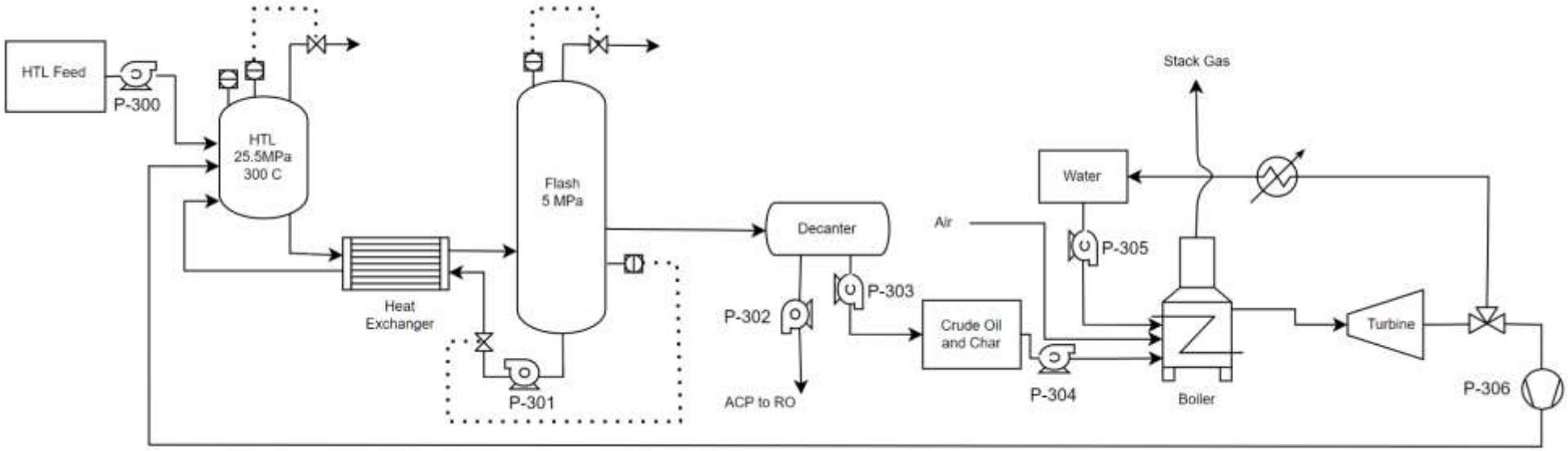

Figure 9.1.1 Process flow diagram of the hydrothermal liquefaction and power cycle systems.

9.2 Feedstock Characterization

The Cooum River is heavily polluted with raw sewage, trash, agricultural waste, and industrial effluent (Gowri et al., 2007). Streams of these pollutants discharge into the river daily, however the exact amount of waste in the river is unclear. Furthermore, Chennai has a tropical maritime climate, which supplies a wet monsoon season. The characteristics of the waste in the Cooum River, including concentrations and mass flow rates, change from pre to post monsoon season (Gowri et al., 2007). There are two streams of waste from the Cooum River that will feed HTL: large solid waste collected from the mechanical prescreen, and smaller solid waste from the underflow of sedimentation. In addition to the river waste streams, the HTL feed will be supplemented with raw sewage imported by local sewage collection trucks. India is a developing country, and this context is important to consider when estimating available volume of feed into the reactor. In Chennai thousands of residential homes and apartment complexes are not connected to the underground drainage network, and instead hire private trucks to carry away sewage (Srinivasan, 2017). The cost of this service is between 750 - 1000 rupees, or 10 - 13.5 USD (Srinivasan, 2017). Furthermore, many trucks illegally dump the sewage to avoid the ₹100 (1.33 USD) fee to discharge the water at a treatment plant (Srinivasan, 2017). As sewage is a profitable HTL feed, removing any discharge fee provides a reliable, and free, source of feed to mitigate river flow rate uncertainties. Each of these trucks can carry up to nine m^3 of sewage in one trip, and will make up to 10 trips a day, which greatly exceeds the required feed for one batch a day (Srinivasan, 2017).

The high variability of the daily feedstock for HTL provides a significant challenge to predict the mass flow rate as well as the composition of the feed. The expected daily flow rate from sedimentation was previously calculated to be a maximum of 0.38 m^3/day during the pre-

monsoon season, as can be seen in Section 5.2, Table 5.2.1. The flow rate of the larger solids from the pre-screen is unknown, as no literature was found containing the larger waste present in the river. The flowrate of the supplemental sewage collected from private companies depends on both the flow rates of the pre-screen and the sedimentation tank underflow. Enough sewage will be imported as required to make up a complete batch for the HTL reactor. To ensure there is enough feed for a batch a day, all of the feed streams to the reactor will first enter a collection/holding tank until required for the next batch.

Both the composition and mass flow rate largely impact the products from the HTL reaction, so it is important to characterize the feedstock before moving on with reactor design and batch scheduling. If this project were to be designed for further consideration, a detailed investigation into the solid waste contaminants of the Cooum River over the course of a year is highly recommended.

In order to characterize the feedstock, various assumptions are made:

1. The solids that will be captured for HTL consist of: raw sewage sludge, municipal garbage (both degradable and nondegradable), and agricultural waste (Gowry et al., 2007).
2. Enough solid waste will be collected in a collection tank to supply one batch reaction a day as a result of collection from the river and supplemented imports of raw sewage from local trucking companies.
3. The average oxygen to carbon atomic ratio, hydrogen to carbon atomic ratio, and ash content of these components can be used to characterize a general feedstock mixture. These values are listed in Table 9.2.1.

4. The feedstock mixture from the Cooum River can be accurately represented by the feedstock group ‘biodegradable waste’ as assigned from the machine learning models by Cheng et al. in their research of hydrothermal treatment.

Table 9.2.1 Characteristics of the dominant contaminants of the Cooum River.

	Raw Sewage Sludge	Municipal Garbage	Agricultural Waste
O/C atomic ratio	0.820	0.509	0.556
H/C atomic ratio	1.630	1.496	1.612
Ash Content (%)	39.200	6.697	8.244

The research carried out by Cheng et al. was used to characterize the feedstock as well as output yield at various HTL conditions. This research used machine learning to combine and analyze data from approximately 70 studies of HTL with various feedstocks to predict the effect of feedstock composition and reactor temperature on product yields, energy content, and carbon content (Cheng et al., 2020). Using Figure 9.2.1, below, and the oxygen to carbon ratio, hydrogen to carbon ratio, and ash content of the contaminants known to be at high levels in the Cooum River, the characteristics of the Cooum River feedstock were estimated to most closely match those of the feedstock ‘biodegradable waste’ assigned by Cheng et al.

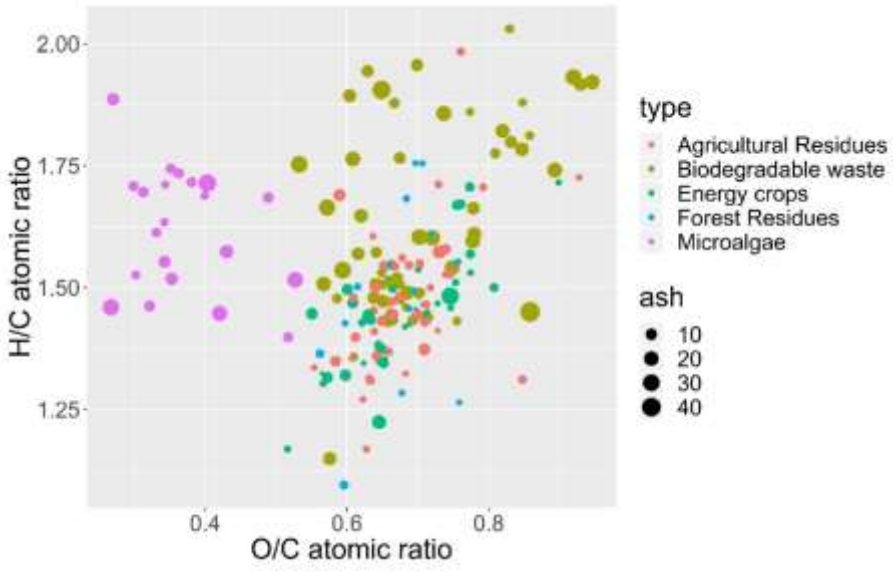

Figure 9.2.1 The O/C atomic ratio, H/C atomic ratio, and ash content of selected feedstocks. (Cheng et al., 2020)

The chemical compositions of the products vary as the feedstock to the reactor changes, however the general characteristics can be defined. Bio-crude oil is the highest energy product, and is defined as a liquid fuel derived from biodegradable waste. Similar to crude oil, bio-crude consists of a mixture of oxygenated organic compounds with a wide molecular weight range (Crocker, 2010). Bio-crude oil can be further processed and separated to produce purified oils for fuel, however in the following process the oil is being burned immediately after production further processing is not carried out. The second high-energy product is the char produced, or the solids from the reactor. Like the bio-crude oil, the char produces is similar to charcoal in composition and energetic properties, but made from biodegradable matter (Crocker, 2010). There is a wide variety of gasses produced by HTL, and little research has been carried out to determine the overall composition. The gasses produced likely include: carbon dioxide, carbon monoxide, methane, ethane, ethene, propene, propane, and butane (Zhang et al., 2018). Carbon

dioxide is likely produced the most of these gasses. The last product is the aqueous co-product, which consists of water as well as any small particle, suspended solids from the reactor.

9.3 Material Balance

Based on the feedstock characterized prior, Cheng et al. was used to assume yields based on biodegradable waste. The yields provided in Figure 9.3.1 are averages on a weight basis and were scaled to add up to 100%, as mass must be conserved for reactor input and output streams. The numerical yields can be seen in Table 9.3.1.

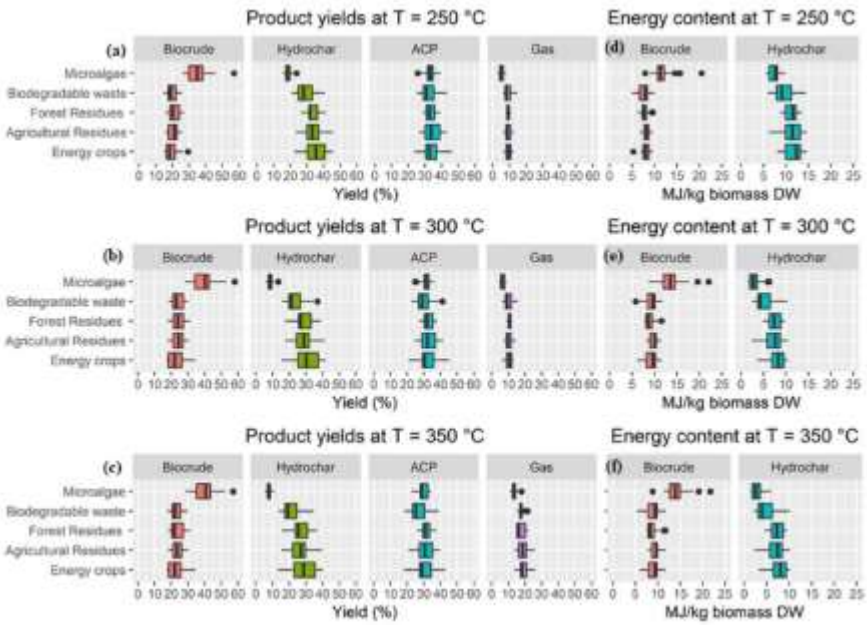

Figure 9.3.1 Yields and energy content for selected feedstock at different temperatures. (Cheng et al., 2020)

Table 9.3.1 Product varieties and their scaled yields.

Product Type	Yield (wt%)
Bio-crude	0.2875
ACP	0.3375
Gas	0.1125
Char	0.2625

In the design of the reactor, a 10 m^3 reactor size is to be used with a batch size of 5.2 m^3. This batch size, when assuming a feedstock density of 1060 kg/m^3, will be 5506 kg (Dammel & Schroeder, 1991). The product masses and volumes can be seen in Table 9.3.2. The masses are conserved, while the volume dramatically increases due to the volume of the gas product. This gas will be vented from the reactor using a flash drum vapor separation system (See Section 9.5). This will help to regulate the pressure within the reactor. The three other products, bio-crude oil, char, and ACP, are all sent in one stream to the centrifugal decanter.

Table 9.3.2 Product yields in mass and volume basis.

Product Type	Mass Yield (kg)	Volume Yield (m^3) STP
Bio-crude	1583	1.60
ACP (including steam injection water)	1858	6.70
Gas	619	512.00
Char	1445	0.64

9.4 Batch Scheduling

The primary goal of the HTL reaction is to produce as much energy as possible to supply the electricity required to carry out RO. This energy requirement was the largest factor in determining batch sizing and schedule. The estimated requirement for the pumping of water for RO is approximately 766.29 kW for the pre-monsoon season and 517.92 kW for the post-monsoon season. Using the lower heating value of the bio-crude oil and char products, a batch size of 5.2 m^3 was determined to achieve approximately 301 kW, accounting for a 75% efficiency loss during electricity generation. Using these estimations, the planned batch schedule is one 5.2 m^3 batch a day. As the reaction is very dirty, there will be an inevitable accumulation of solids on the interior of the reactor, including char and ash. Because the reactor is only being used once a day, cleaning will occur between batches when necessary.

Each batch will take approximately three hours to complete the reaction. During the first two hours the reactor will be gaining temperature and pressure, and should reach reaction conditions within that time. The reactor will maintain reaction conditions for one more hour, which is estimated to be enough time for all of the feed to fully react. The products will then be

pumped out of the reactor into a decanter to be separated. This timeline is an estimate based on reviewed literature, however, further experimentation is recommended to better understand the reaction kinetics and the time required to complete the reaction.

9.5 Reactor Design

The reactor itself is an isothermal baffled batch reactor using direct steam injection to provide heat. Due to the sewage feed not being continuous and being variable day to day, a batch type reactor is used. The reactor is cylindrical with a rounded bottom. Additionally, the reactor is to be kept at 300℃, and uses an impeller and baffles to provide agitation and guarantee uniform temperature throughout the reactants. The yield values and energy content values are based on data accumulated at 300℃ in Cheng et al. (2020), so that temperature is to be used in the reactor. The reactor is also kept at 25 MPa, as this is suggested to be an optimal value for HTL reactors (Castello et al., 2018).

The size of the reactor was determined using the following system of equations:

$$L/D = 3 \tag{9.5.1}$$

$$A = \pi D^2/4 \tag{9.5.2}$$

$$A * L = 9 \tag{9.5.3}$$

Equation (9.5.3) assumes that one m^3 is accounted for in the rounded bottom of the reactor. These equations were solved simultaneously in MATLAB, and provided the required length and diameter of the reactor based on an L/D provided by Perry's Handbook and the reactor's volume

limitations. The length and diameter of the reactor is 4.69 m and 1.56 m, respectively. The wall thickness was chosen to be 1” to match standard values for wall thickness.

A Rushton impeller at 500 rpm was chosen because the Rushton is used commonly for gas dispersion and the agitator speed is standardly used for HTL reactors (Ovsyannikova et al., 2021). The impeller is 0.7 m wide, based on ratios presented in Perry’s Handbook. Baffles were also chosen to be added as they promote axial mixing that would not be accomplished using the radial Rushton impeller (Yu et al., 2015). A full diagram of the reactor can be seen below in Figure 9.5.1.

Due to the constant generation of gases in the supercritical mixture within the reactor, those gases must be continuously separated and treated. A flash vapor-liquid separator will be used to extract out generated gases while feeding all liquid products back into the reactor. The composition of this gas can be seen in Table 9.5.1 (Tzanetis et al., 2017). The feed will be circulated at a mass flow rate of 10% every minute, so that the full contents of the reactor get recirculated six times per hour. There are many aspects of the HTL reaction that are uncertain but affect the reactor and flash drum design, specifically reaction kinetics and the volumetric rate of gas produced. As a result, there is significant uncertainty in how to design this reactor system at a large scale. The 10% recycle flow rate is an estimate of the required rate to prevent the reactor from overpressurizing as a result of gas production. An in-depth study of the reaction kinetics and gas production is highly recommended for more accurate flow rate calculations.

The recycle stream is fed to the flash drum after passing through a heat exchanger (See Section 9.6). The flash drum is operated at 5 MPa and 69℃ for vapor formation below the

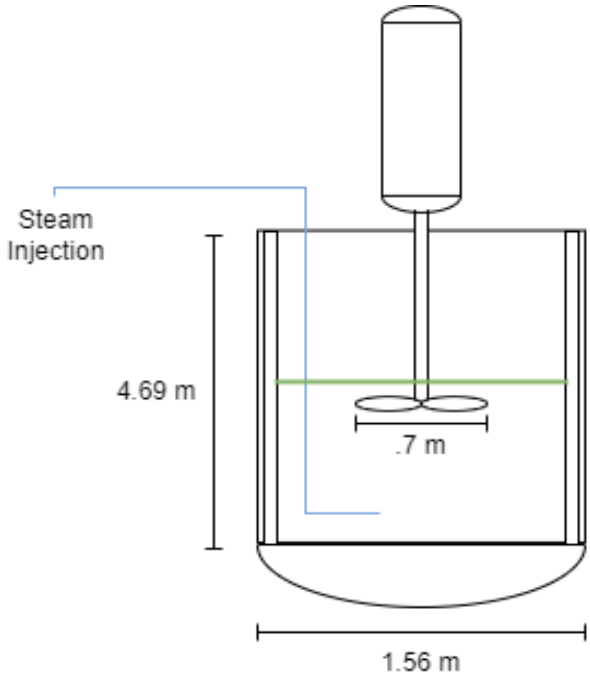

Figure 9.5.1 HTL reactor dimensions and steam injection.

critical pressure and temperature of CO_2 (7.3 MPa). A pressure gauge measures the pressure in the flash drum and controls a valve to release gases from the drum when necessary to maintain drum pressure. The drum size was determined to be 5.7 m in diameter and 17 m tall with a mesh deentrainer to form large droplets that will separate from the gas phase. The sizing was calculated using formulas found in flash design material from the University of Oklahoma, assuming the following equations for permitted velocity and diameter:

$$v_{perm} = k\sqrt{\frac{\rho_L - \rho_V}{\rho_V}} \tag{9.5.4}$$

$$D = \sqrt{\frac{4V}{\pi v_{perm}\rho_V}} \tag{9.5.5}$$

Equation (9.5.4) can also be seen in Peters & Timmerhaus “Heuristics for Process Equipment Design”, stating that k, a separations constant, can be assumed to be 0.1 with a mesh deentrainer. When plugging in V as the vapor flow rate, a calculated v_{perm} using densities found , and the density of the vapor into Equation 9.5.5 the diameter results in 5.7 m. Using an optimum length/diameter ratio of 3, the height of the drum would be 17 m high.

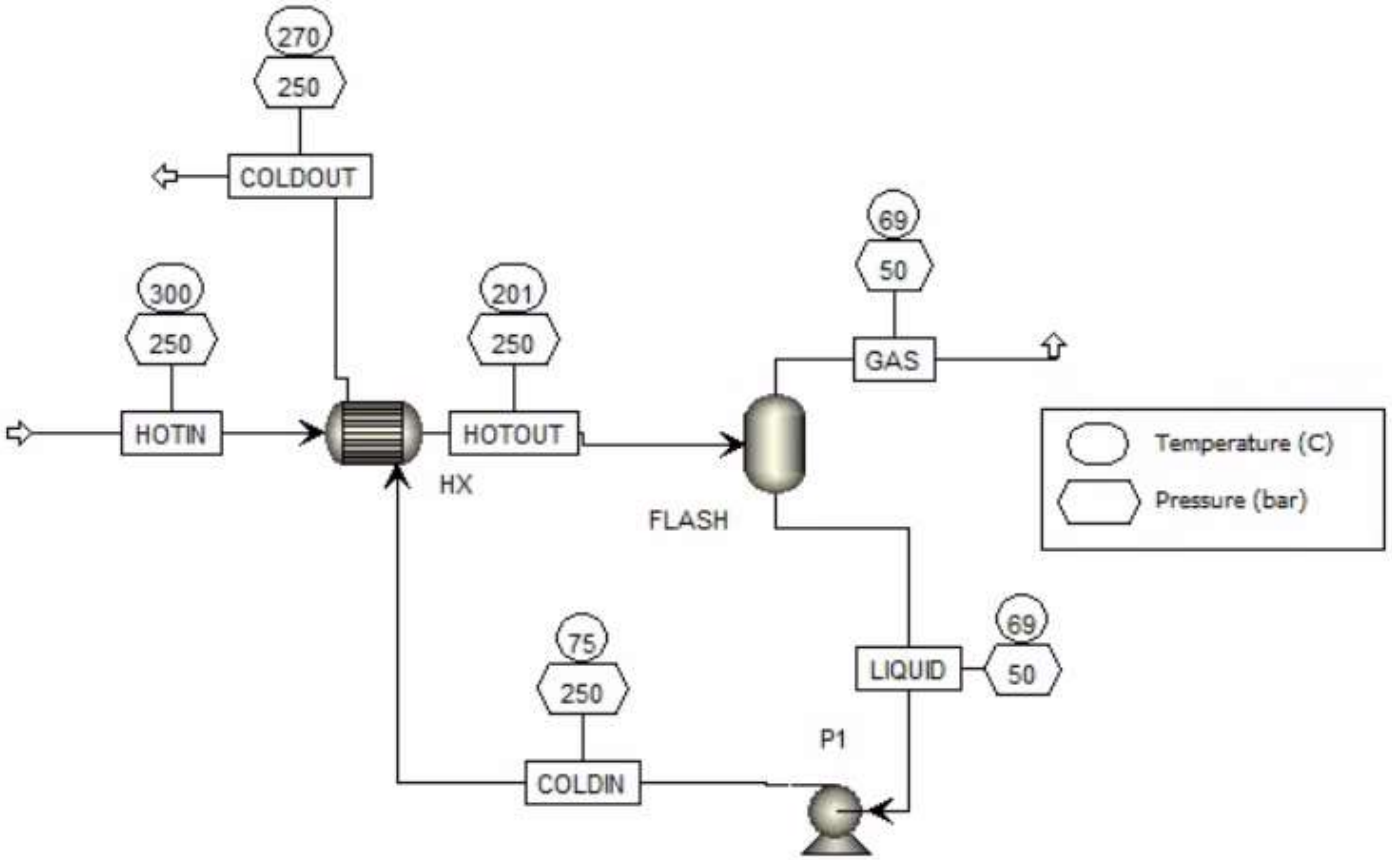

Figure 9.5.2 Aspen model of flash and heat exchanger system for gas extraction from reaction mixture. Modeled eicosane, water, carbon monoxide, and carbon dioxide using Predictive SRK

9.6 Heat Equipment

Direct steam injection is used to heat the reactor. The reactor volume is 10 m^3, so with such a high volume to surface area ratio, a heating jacket on the outside of the tank would not be effective. Direct steam injection has many benefits to this process. First, the steam input into the reactor will either condense and leave as ACP, take part in the reaction, or leave as a gas from the flash drum. Because of this, it integrates very well with the reactor and subsequent separations. Second, the heat transfer efficiency from the steam to the reactants is very high, as there is no tertiary material between the steam and the reactants to be heated. Third, the water purchased for steam will have a net negative cost as it will be recycled and cleaned through reverse osmosis to be cleaned then sold. Fourth, injecting steam at the bottom of the tank will increase mixing in the tank as the steam rises and mixes in the reactants.

An automatic valve will control the steam flow rate into the reactor based on a temperature gauge. Superheated steam will enter the reactor at 25.5 MPa and 300℃ (573 K). The heating time to reach the reaction temperature is two hours, and the reactor will be held at reaction conditions for an hour for a total of three hours. An estimated steam flow rate to heat the reactor from 25 to 300℃ (298 to 573 K) and maintain this temperature was calculated to be about 1600 kg/h. This calculation includes the mass flow rate of steam to heat the reactor contents, as well as the heat that will be lost to heat the steel reactor and heat loss from the reactor to the surrounding air.

Equations (9.6.1) - (9.6.4) were used to calculate the heat transfer and steam mass flows into the reactor:

$$\dot{m} = \dot{Q} / (h_g - T_f * c_p) \quad (9.6.1)$$

$$\dot{Q} = (m * c_p * \Delta T) / t \quad (9.6.2)$$

$$\dot{Q} = U * A * \Delta T \quad (9.6.3)$$

$$\dot{m} = \dot{Q} / h_g \quad (9.6.4)$$

where $\dot{m}$ is the mass flow rate (kg/h), $\dot{Q}$ is the heat transfer rate (kW), h_g is the specific enthalpy of steam at 25.5 MPa and 648K (1842.35 kJ/kg), T_f is the set reaction temperature (573 K), c_p is the heat capacity of the HTL feed (1.25 kJ/kg K) and 316 stainless steel (0.49 kJ/kg K), U is the overall heat transfer coefficient of the steel reactor (13 W/m^2 K) and A is the outer area of the reactor (26.8 m^2).

Equation (9.6.1) was used to calculate the mass flow rate of steam to heat the biodegradable waste and tank. The heat transfer rates to the biodegradable waste and surrounding steel tank were calculated using (9.6.2). The heat loss from the tank to the surroundings and the mass flow rate of steam to supplement the heat were calculated using (9.6.3) and (9.6.4), respectively. The mass flow rates of steam were then summed to achieve the total flow rate of 1609.0 kg/h. Feedback loops will be used to control the flow of steam in, to heat the reactor, and the flow of gases out, to remain at a pressure of 25MPa. These pressure and temperature gauges connected to steam and gas flow rates can be seen in Figure 9.6.1, below.

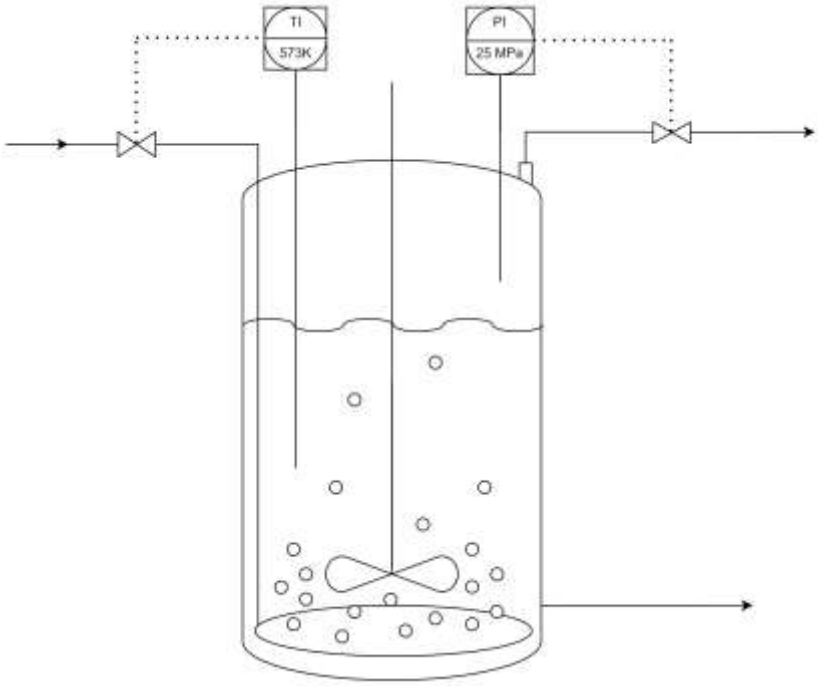

Figure 9.6.1 Reactor with temperature and pressure feedback loops.

The design of the direct steam injection valves, temperature controller, and pressure controller are out of the scope of this project.

A shell and tube heat exchanger is used to conserve heat leaving the reactor that would otherwise be lost in the rapid expansion that occurs in the flash drum. The stream leaving the reactor is at a temperature of 300°C, and leaves at a temperature of 201°C. This heat is transferred to the stream out of the flash tank traveling towards the reactor, which enters the heat exchanger at 75°C and leaves at 270°C. The 30°C temperature difference between the stream entering the reactor and the 300°C reactor will be made up by increasing the direct injection steam flow rate, controlled by the temperature controller. A design of this heat exchanger (along with the flash drum) was created in Aspen Plus, the flowsheet of which can be seen below. This design specifies a heat exchanger area of 102 m^2. The exchanger was assumed to be run

countercurrent, with the hot fluid flowing through the tube due to the higher temperature feed (Peters et al., 2002, p. 970).

9.7 Separations

The product stream exiting the HTL reactor is an emulsion of ACP and bio-crude oil with suspended char particulates. To recycle the ACP, the majority of the char and oil must be removed. In addition to cleansing the ACP for microfiltration, the separation process creates a more efficient fuel source to use in the furnace. Other projects have used a variety of separation methods to remove water from bio-crude oil. These methods include extraction, gravity separation, and coalescence (Gupta et al., 2017). For this particular water treatment facility, none of the aforementioned methods are suitable. Extraction involves the introduction of harsh chemicals that would consequently need to be removed from the water later in the treatment process (Gupta et al., 2017). This complicates the process, adds costs, and produces more waste. Gravity separation eliminates additives, but is too time consuming (Gupta et al., 2017). It would not allow for daily fuel production for RO. Coalescence involves sensitive fiber cartridges that would disarm if small amounts of char are fed into the separator (Pall Corporation, 2022). This would require frequent maintenance and expensive upkeep.

To achieve effective separation, while forgoing chemicals and minimizing maintenance costs, HTL product separations are carried out using a three phase centrifugal decanter. This decanter functions similarly to a sedimentation tank wrapped around an axis. The HTL emulsion is fed through the center of the rotating chamber, as seen in Figure 9.7.1. The walls of the chamber will be moving at approximately 3,000 rpm (Flottweg Separation Technology, 2016). The centrifugal force induced from the rotation causes the dense char particles to collect on the chamber walls. The center scroll rotates at a lower speed than the walls, allowing it to act as a conveyor for the char solids (Flottweg Separation Technology, 2016). The scroll scrapes the char particulates off the wall and slowly pushes them to the outlet, effectively separating them from

the liquids and producing a dry product. The oil and water continue to separate as the solids move to the opposite end of the chamber. The light liquid, or oil, remains closest to the axis of the cylinder. As a result, it is skimmed off the top using a baffle (shown at the top of the chamber in Figure 9.7.1). Likewise, a baffle oriented in the opposite direction pulls the heavy liquid, ACP, out of the mixture at the bottom of the chamber.

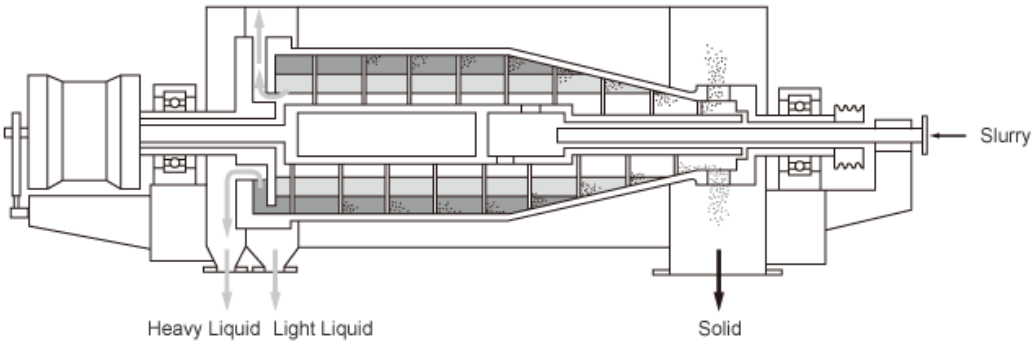

Figure 9.7.1 Cross section of three phase centrifugal decanter. (IHI, 2022)

The particular model that will be used for HTL separations will be the Flottweg Z3E Decanter. This decanter has a maximum hydraulic capacity of 15 m^3/h, meaning that the decanter will be able to easily handle the daily load of 6.36 m^3 HTL emulsion (Flottweg Separation Technology, 2016). Additionally, this decanter is compact compared to similar units, and has a total footprint of 2.95 m by 0.84 m (Flottweg Separation Technology, 2016). Furthermore, the separation using the Z3E decanter is excellent, and can be refined during operation using the Simp Drive®. The Simp Drive® allows for adjustments to be made to the rotation speeds of the chamber and scroll, in order to find the optimum settings for maximum separations. The minimum separations guaranteed from the unit can be seen in Figure 9.7.2. Overall, the oil stream will be less than 2% ACP and less than 0.3% char (Flottweg Separation Technology, 2016). Assuming that only the minimum separation is achieved, HTL would produce 2,802.8

kg/day ACP to be recycled, as well as 2,223.31 kg/day char and 2,503.89 kg/day bio-crude oil to be sent to the furnace.

Figure 9.7.2 Material balance for HTL separations.

After the bio-crude oil, char, and ACP are separated, the oil and char are pumped to the same tank, which is agitated to suspend the char in the oil to create a relatively homogeneous mixture of oil and char. A mixture of oil and char is required as feeding a stream of pure char in its solid form would not burn in the boiler without incineration. The agitation will also break up the char into smaller pieces which is required to maintain consistent flow into the reactor and also supports efficient burning. By creating a fluid input stream to the boiler, rather than alternating between solid and liquid, the flow rate can be controlled and the mixture will burn relatively consistently to supply a steady flowrate of steam out of the boiler. After burning, the

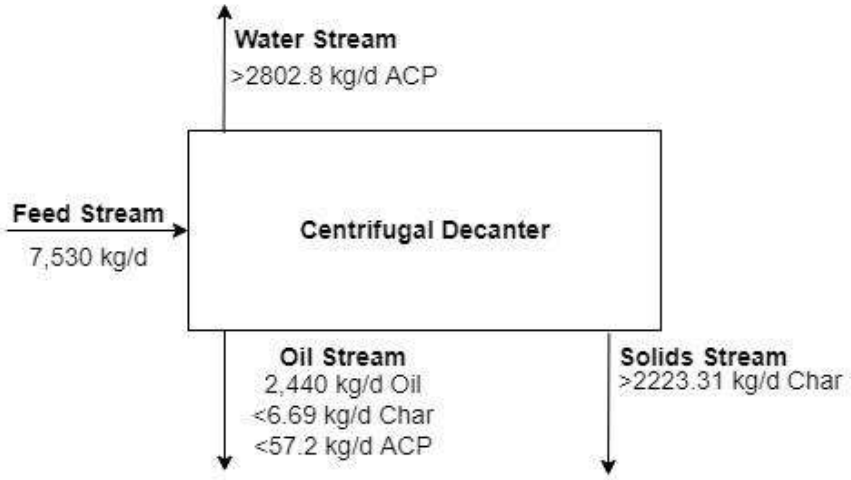

char will produce ash which will likely cause blockages in the boiler system. Therefore, two boilers will be installed, and will be used alternatively when the inevitable cleaning and repairs of the operating boiler are required.

9.8 Power Cycle Design

In order to produce usable energy from the high-energy products of HTL, specifically the bio-crude oil and the char, a steam turbine is used. RO requires a constant supply of energy, however the HTL reaction is carried out in batches which means the energetic products are only collected once a day. To supply energy at a constant rate, the bio-crude oil and char will be collected into a holding tank after HTL and separations, and fed at a slower rate into a boiler to produce a constant stream of steam. This hot steam will then run through a turbine to produce electricity that will directly be sent to RO. The steam will then flow through a condenser where it will drop in temperature, condense, and be sent to a holding tank before the boiler. While the HTL reaction is occurring, however, the steam will instead be sent from the boiler directly to the HTL reactor to provide heat to the reaction. A three way valve and switch will be used to control the direction of the steam flow. The design of the valve and switch is out of the scope of this project.

This power cycle can be seen in the two flowsheets below, both of which were designed in Aspen Plus. Figure 9.8.1 depicts the power cycle operating when the HTL reactor is not operating. Figure 9.8.2 depicts the power cycle operating while the HTL reactor is operating. In both cases, the water entering the boiler has a temperature of 25^{o} C, a pressure of 100 bar, and a flow rate of 9.89 m^3/hr. Leaving the boiler is a 380 m^3/hr superheated steam, at a temperature of 600^{o} C and pressure of 100 bar. The superheated steam enters the turbine where it generates 301 kW of power. This electrical power produced will be used to help power the pumps for reverse osmosis. The steam exiting the turbine flows at 1410 m^3/hr with a temperature and pressure of 366^{o} C and 20 bar respectively. When the HTL reactor is not operating, the steam out of the

turbine will flow to the condenser where it will be condensed to 25^{o} C and 5 bar and will flow into the utility water holding tank.

During the HTL reactor operation, the stream exiting the turbine flows into a compressor to be pressurized to 250 bar and 875^{o} C. This steam is injected into the reaction vessel heating the reactor to operating temperature and maintaining the reactor temperature during the reaction. The steam flow rate into the reactor is controlled using a temperature sensor and controller, the design of which is out of the scope of this project.

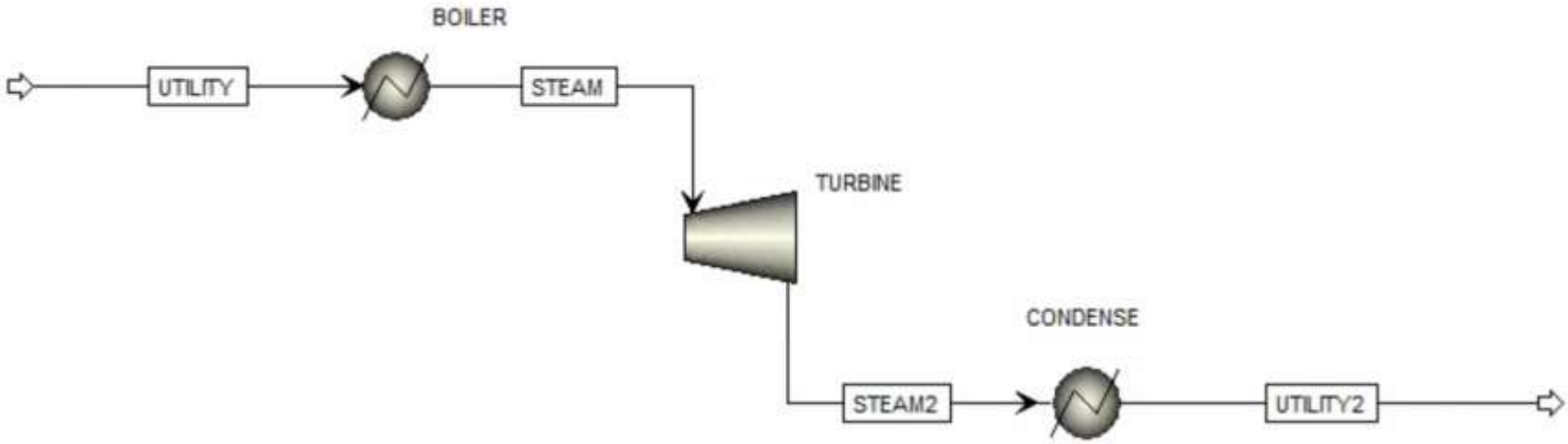

Figure 9.8.1 Power cycle sequence when the HTL reactor is not operating. Modeled in Aspen using water as the component and the NBS/NRC steam tables property method.

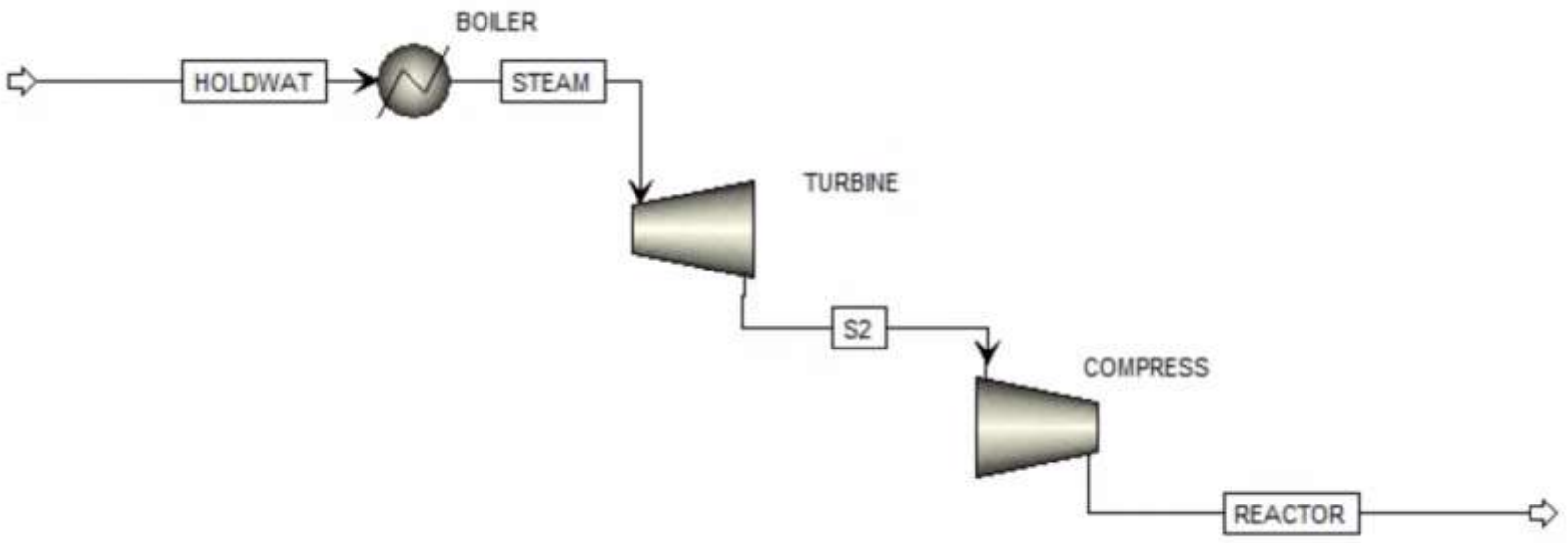

Figure 9.8.2 Power cycle sequence when the HTL reactor is operating. Modeled in Aspen using water as the component and the Steam Table property method.

9.9 Pump Requirements

Pumps are an important feature to the HTL and power cycle. The most power intensive pumps only operate for three hours a day, during the HTL reaction. These pumps are moving the liquid bottoms of the flash and the steam leaving the turbine into the reactor from a low pressure up to 25.5 MPa, and are labeled as P-301 and P-308 respectively. The large pressure difference from both the boiler and the flash to the HTL reactor is what creates the high power requirement of said pumps. These power values were calculated using heuristics, and the power requirement of the two largest pumps, P-301 and P-308, were confirmed by Aspen Plus. A 75% efficiency was assumed for all pumps.

The calculated pumping requirements are tabulated in Table 9.9.1, below. The pressure difference includes frictional losses that occur from pipes, heat exchangers, condensers and valves. Power values are tabulated including a 75% efficiency assumption.

Table 9.9.1 HTL and power cycle pumping requirements.

Pump	Volumetric flow rate (m^3/s)	Pressure difference (MPa)	Power (MW)
P-300	$6.37x10^{-2}$	0.25	$2.12x10^{-2}$
P-301	$1.23x10^{-2}$	30.60	$5.04x10^{-1}$
P-302	$3.12x10^{-3}$	0.25	$1.04x10^{-3}$
P-303	$1.05x10^{-3}$	0.25	$3.50x10^{-4}$
P-304	$2.63x10^{-5}$	0.25	$8.76x10^{-6}$
P-305	$2.75x10^{-3}$	10.10	$3.72x10^{-2}$
P-306	$5.65x10^{-2}$	27.60	$2.08x10^{0}$
Total			**2.62**

10. Final Design

The recommended design of a water treatment plant in Chennai, India, to provide potable water using reverse osmosis and supplement energy usage with hydrothermal liquefaction is as follows:

Approximately 13,300 m^3/day is pumped from the Cooum River and is immediately sent through a mechanically cleaned Raptor® FalconRake® Bar Screen. This screen will remove any objects above the diameter of 6 mm which will be collected into a collection tank and directly transferred to the hydrothermal liquefaction reactor when full.

The water flows through the screen into a series of sedimentation tanks, where 86% of all particulates will be removed from the water. The series of tanks allows for additional settling time and holding capacity, ensuring that both the microfiltration and reverse osmosis equipment are protected from excessive pollution during times of increased solids concentration. The feed will be directed to one of two circular, radial flow clarifiers before moving to a rectangular, horizontal flow clarifier. The pair of circular sedimentation tanks will operate with a 3.43 hour detention period and 28 $m^3/(day*m^2)$ surface overflow rate. The rectangular tank will operate with a 4 hour detention period and 24 $m^3/(day*m^2)$ surface overflow rate. The settled particulates will be mechanically scraped off the bottom and transferred to the hydrothermal liquefaction reactor on a daily basis. The overflow, consisting of river water containing dissolved solids and non-settleable particles, will be pumped to microfiltration for further processing.

The overflow is divided into parallel microfiltration units so it can all be processed at once. The filters remove all suspended solids and greatly reduce BOD and COD concentrations at an applied feed pressure of 2.03 bar. Neglecting frictional pressure loss along the membrane,

the retentate is pumped from a pressure of 2.03 bar to a higher pressure for reverse osmosis. With a pressure drop of 0.03 bar, the permeate will flow at an applied pressure of 2 bar. Twenty four Microza* Hollow Fiber UNA microfiltration modules placed in parallel each with a length of 2.16 m will be used to achieve a permeate flow rate of 12,672 m^3/day. The hollow fibers remove all particles with diameters greater than 0.1 μm. A 632.5 m^3/day retentate stream is sent to the hydrothermal liquefaction reactor collection tank.

Three stages of reverse osmosis are recommended to sufficiently clean the water to Indian Standard Drinking Water Specifications (Bhavan, 2012). Pressurized water from microfiltration is pumped to stage 1, where it is divided into 25 pressure vessels to be processed all at once. The retentate is then sent to stage 2, where it is divided into 13 vessels to be processed. The retentate is collected from this stage and sent to stage 3 (containing 6 pressure vessels). While the retentate of stage 3 is dumped into the ocean, the permeate water from each stage is collected and treated by UV light. While one vessel is present to obtain permeate water for backflushing, one vessel is being backflushed with permeate water in a continuous cycling process. Membranes are also continuously cleaned with the recommended chemical $Na_2S_2O_4$.

Depending on the season, some of the operating pressures of reverse osmosis will be affected based on the concentration of TDS in the water. In the pre-monsoon season, water from microfiltration at a pressure of 2.03 bar will be sent to stage 1 at a pressure of 27.61 bar. The retentate will be pressurized up to 47.63 bar to be sent to stage 2. Lastly, the retentate of this stage will be collected and pumped up to 59.38 bar to go through stage 3. Neglecting frictional pressure loss along the membranes, the retentate coming off of stage 3 will be collected at 59.38 bar. This pressure should provide sufficient driving force to move the retentate to the ocean.

During the post-monsoon season, water from microfiltration at a pressure of 2.03 bar is sent to stage 1 at a pressure of 20.32 bar. Retentate water is then pressurized up to 33.51 bar to be sent to stage 2. Lastly, retentate water is pressurized up to 35.72 bar to be sent to stage 3. The retentate water coming from stage 3 is sent at a pressure of 35.72 bar to be sent to the ocean. For both seasons, permeate water is all collected at 2 bar. Since this water has a low salt concentration, the pressure should be sufficient to push water to UV treatment using valves.

The reverse osmosis process makes use of Dupont spiral wound reverse osmosis membranes. The membranes in stage 1 consist of brackish water membranes (99.0% salt rejection) due to the low concentration of TDS in the feed. The higher feed concentrations of TDS mean that stages 2 and 3 contain seawater membranes (99.8% salt rejection). Both of these membranes are 1.016 m long with an outer diameter of 0.201 m and pore sizes of approximately 0.001 microns, allowing for 7 membranes to fit into a single pressure vessel. For both seasons, a total of 12,672 m^3/day is fed into stage 1. With a permeate flux of 40 m^3/day for brackish water membranes and a permeate flux of 28 m^3/day for seawater membranes, the overall permeate flow rate is 10,724 m^3/day (84.63% recovery). The retentate flow rate from stage 3 is 1,948 m^3/day.

The permeate collected from reverse osmosis will be pumped to two SUV---1398 Industrial UV Sterilizers from Pure Aqua. The sterilizers assume 94% UVT, with a dose level of 30 mJ/cm^2 after 375 days of operation. With a combined maximum flow capacity of 15,240 m^3/day, both systems will easily handle the production demands while completely eliminating total coliform bacteria and any remaining viruses or protozoa.

To supplement the high energy usage of reverse osmosis, a hydrothermal liquefaction reaction will be carried out using the wet solid wastes collected from screening, sedimentation, and microfiltration. A 10 m^3 isothermal, baffled, batch reactor will carry out one 3 hour batch a

day of 5.2 m^3 of wet solids. A temperature of 300°C will be maintained using direct steam injection estimated at 1609 kg/h of steam, and a pressure of 25 MPa. A temperature gauge and controller will determine the exact flowrate of steam into the reactor to maintain temperature. The reactor will take 2 hours to heat to the reaction conditions, and the reaction will be complete after 1 hour to produce water, char, bio-crude oil, and gases. Gases are produced at very high volumes during the reaction. To maintain a pressure of 25 MPa, during the reaction 10% of the reactor contents will be cycled through a 5 MPa flash drum every minute to vent the gases. This is necessary as the reactor will be at supercritical conditions so a lower pressure is required for the gas to phase separate from the rest of the reactor contents. A shell and tube heat exchanger will conserve most of the heat lost from the stream leaving the reactor to the flash drum and transfer it back to the stream re-entering the reactor.

A Flottweg Z3E Decanter is used to separate the water from the char and oil which will both be sent to an agitated holding tank. The wastewater from the reaction is pumped to the microfilter for further purification. The mixture of oil and char will be fed to a boiler to produce superheated steam. The steam will flow through a turbine, generating electricity for RO. Each batch is expected to produce approximately 301 kW of energy, supplementing approximately half of the energy required by RO per day. During the HTL reaction, the steam will be compressed and sent to the HTL reactor for direct steam injection. When the HTL reactor is not operating, the steam will be condensed, collected, and sent through the boiler again.

11. Economics

11.1 Capital Costs

One of the most important factors in understanding the economics of the water treatment plant is the estimation of capital cost. Capital costs include the physical equipment needed for the process as well as the land, piping, and cost of installation. For the process, this includes the bar screen, the sedimentation ponds and equipment, the HTL reactor and separation equipment, the microfiltration and RO systems, the UV disinfection equipment, and all the pumps needed. The capital cost of the majority of the equipment is estimated using the 2017 Capcost Excel Sheet modeled from equations found in the Turton textbook (Turton et al., 2016). The Bare Module Cost of each section in the process is then multiplied by the Lang Factor of 4.61 to account for the rest of the piping, land, and installation costs required for the process. The Lang Factor was chosen from Turton et al. for a fluid treatment plant. The total Bare Module Cost for the process is $57,120,950. When multiplied by the Lang Factor, the total capital cost for the process is approximately $263,327,600. The breakdown of the capital cost for each part of the process is described in the sections below.

11.1.1 Screening and Sedimentation

The capital cost of the mechanically cleaned bar screen was estimated using Capcost. Modeled as a stationary screen with a screen area of 2 m^2, the bar screen was estimated to cost $16,400. Adding in a spare bar screen and accounting for installation costs, the cost of the bar screen was estimated to be $43,900 for 2017 pricing. Using the Chemical Engineering Plant Cost

Index (CEPCI), the cost of the bar screen was adjusted to match 2021 pricing. The final capital cost of the bar screen is $57,350.

The capital cost of sedimentation tanks must be determined on an individual basis, due to the lack of uniform specifications across the industry. Equations published by the University of Texas were used to determine the cost of each sedimentation tank needed in the treatment process (Sharma, 2010). These equations, published within a thesis outlining the development of a preliminary cost estimation method for water treatment plants, are the most recent available data that is applicable to the operation in Chennai.

Separate equations were used for the cost estimation of the circular and rectangular sedimentation tanks, shown below

$$CC_C = -0.0005x^2 + 86.89x + 182{,}801 \quad (11.1.1)$$

$$CC_R = -0.0031x^2 + 155.61x + 78{,}329 \quad (11.1.2)$$

where CC_C is the capital cost of a circular clarifier, CC_R is the capital cost of a rectangular clarifier, and x is the surface area of the tank in ft^2. The equations used were developed as general cost equations for water treatment plants moving 1 to 200 mgd of water. The proposed plant in Chennai processes just over 3.5 mgd, and the prices were determined accordingly.

After the costs for the tanks were determined for 2010 pricing, the CEPCI was used to adjust the cost to match 2021 pricing. The rectangular sedimentation tank has a surface area of 6,725 ft^2, and the current cost is $1,265,700. The circular sedimentation tanks have individual

surface areas of 5,764 ft^2, and the current individual cost is $857,500. The combined capital cost for the sedimentation process is $2,980,700.

11.1.2 Microfiltration and Reverse Osmosis

The capital cost of the microfiltration and reverse osmosis systems were estimated together using a cost modeling research paper from the International Desalination Association World Congress in 2011 (Huehmer et al., 2011). The capital cost of the filtration systems are dependent on their capacity. Using a regression modeled capital cost equation,

$$log(cost) = 0.81 * log(capacity) + 4.07 \quad (11.1.3)$$

the capital for the filtration systems was calculated. With a capacity of about 13,300 m^3/day, the capital cost of the entire filtration system is $25,725,000. The capacity of the system is increased by 30% to account for auxiliary membranes and pressure vessels that can replace operating membranes when needed. This added capacity increases the capital cost to $31,815,000. This cost equation was modeled in 2011, so the cost is adjusted using the CEPCI. The final capital cost for the entire filtration system is $38,457,000.

The cleaning system is not included in the filtration system calculation, but should be factored into the capital cost estimate. A 10,000 m^3 holding tank is required to hold the cleaning solution when it is not operating. Using Capcost, this tank was modeled as a 10,000 m^3 storage tank with a floating roof. The estimated Bare Module Cost, which included cost of installation, is $790,000. Adjusting the cost from 2017 to 2021 values using the CEPCI, the final cost of the storage tank is $1,032,000, bringing the total cost of microfiltration and reverse osmosis to $39,489,000.

11.1.3 Hydrothermal Liquefaction and Power Cycle

Hydrothermal liquefaction and the power cycle include several different types of equipment. This equipment includes a reactor, a heat exchanger, a flash drum, a decanter, a boiler, a turbine, and a condenser. The capital cost of all of the equipment was estimated using Capcost. The cost of each is tabulated below in Table 11.1.1.

Table 11.1.1 HTL and power cycle equipment capital costs.

Equipment	Equipment Modeled in Capcost	Bare Module Cost (2021)
Reactor	Autoclave Reactor	$516,000
Heat Exchanger	Floating Head Heat Exchanger	$382,700
Flash Drum	Pressure Vessel	$896,100
Decanter	Centrifuge with Spare	$118,900
Boiler	Process Heater	$4,167,000
Turbine	Axial Turbine	$3,396,300
Condenser	Double Pipe Heat Exchanger	$39,700
Total		**$9,516,700**

11.1.4 UV Disinfection

The capital cost for the chosen UV disinfection system is not available without consultation. Therefore, an estimated cost equation developed by the American Water System in 2001 was used to calculate the pricing of the UV units (University of New Hampshire, n.d.).

$$CC_{UV} = 1{,}766{,}000 + (\frac{86{,}950}{MGD} * MGD_{PLANT\ CAP.}) \quad (11.1.4)$$

where CC_{UV} is the capital cost of the UV system, MGD is the daily flow rate in millions of gallons, and $MGD_{PLANT\ CAP.}$ is the plant capacity in millions of gallons per day. The average flow is approximately 10,052 m^3 or 2.66 mgd. The maximum capacity of sedimentation is 15,000 m^3, making the maximum potential flow for the UV unit approximately 11,325 m^3 or 3.0 mgd. Inserting these values into the equation, and adjusting using the CEPCI, yields a capital cost of $3,347,200. This cost includes all initial lamps, lamp sleeves, and other necessary supplies.

11.1.5 Pumps

The reverse osmosis and hydrothermal liquefaction processes operate at high pressures, so pumping the fluids to these pressures is very important. The capital cost of the pumps in the process were estimated with Capcost with the exception of any pumps operating over 100 bar. The capital cost of those pumps was estimated with Peters & Timmerhaus *Plant Design and Economics for Chemical Engineers*. The capital costs of the pumps are tabulated below in Table 11.1.2. Each pump has a corresponding spare pump which is included in the cost estimation.

Table 11.1.2 Pump capital cost.

Process	Number of Pumps	Bare Module Cost (2021)
Sedimentation	2	$108,700
Microfiltration and RO	4	$882,500
HTL and Power Cycle	7	$738,800
Total		**$1,730,000**

11.2 Operating Costs

In order to estimate the cost of labor required for year round plant operations, the number of operator workers needed per shift was estimated using Equation (11.2.1) from Turton et al.. The equation is as follows:

$$N_{OL} = (6.29 + 31.7 * P^2 + 0.23 * N_{np})^{0.5} \quad (11.2.1)$$

where N_{OL} is the number of operators per shift, P is the number of operation steps that involve processing particulate matter, and N_{np} is the number of operation steps that involve the processing of non-particulate matter. Estimates for the values of P and N_{np} are shown in Table 11.2.1. With these values in mind, the number of operators needed per shift was calculated to be 51.

Table 11.2.1 Estimations of P and N_{np} terms to calculate operator labor needed.

Particulate Process Steps	Count	Non-particulate Process Steps	Count
Sedimentation Tanks	3	HTL Reactor	1
RO Stages	3	UV Treatment steps	1
Microfiltration Steps	1	Turbine	1
Pre-Screening	1	HTL Heat Exchanger	1
Decanter Step (HTL)	1	HTL Furnace	1
		HTL Flash tank	1
Total Steps	P = 9	Total Steps	N_{np} = 6

To determine how much labor would cost every year, the number of operators per shift was multiplied by the "yearly operation" factor. Assuming that each operator works 49 weeks out of the year (accounting for vacation and sick time off) and 5 shifts per week, the number of shifts per year that one operator works is 245 shifts/year. The drinking water plant will be in operation for 364 days during a regular calendar year and for 365 days during a leap year. The plant will be closed one day every year for UV treatment maintenance. For simplicity's sake, all operating cost calculations will be performed with a leap year in mind (365 days of operation/year). Three shifts are needed every day (each lasting 8 hours), so there are 1095 shifts per year that need to be filled by operators. This gives a yearly operation factor of 4.5 (1095/245). Multiplying this by the number of operators needed per shift gives 227 operators needed per year (Turton et al., 2016). A typical yearly salary of ₹2,940,456/year for an

operations engineer in India was taken from an online job board, which is assumed to include benefits and insurance (Indeed, 2022). This equates to a yearly salary of $38,225.93 (using the current year's exchange rate of 0.013 USD = 1 rupee) for one operator, or $8,677,285.66 for yearly operator wages.

In addition to the cost of labor, the cost of utilities was calculated. Power that HTL does not provide in the process is needed. Utility water to make steam to spin a turbine to produce power from energy created from HTL is needed. Lastly, utility water is needed to make the cleaning solution used for the microfiltration filters and RO membranes. It was determined that 30,000 m^3 of water was needed to make enough cleaning solution to last for one year. Accordingly, the mass of $Na_2S_2O_4$ needed to make the solution is the only raw material needed for our process, and the cost of this chemical comes out to $690,000.00. Additionally, it was determined that 10,829.55 m^3 of water was needed to produce steam for the HTL power plant. Using the average price that industries are charged for utility water (27.54 rupee/m^3), the total cost of utility water was estimated to be $14,617.80/year (Express News Service, 2020).

Continued upkeep of the UV disinfection systems requires additional UV lamps, quartz lamp sleeves, and a mild acidic cleaning solution. UV lamps are replaced every year, and 60" models online are typically priced around $420.00 (Aquafine, n.d.-b). The failure rate of the lamps is not mentioned in available resources, and the assumption has been made that the lamps will not need to be replaced outside of standard maintenance. As such, 12 lamps will be purchased per year, at a cost of $5,040.00 (Aquafine, n.d.-b). The quartz lamp sleeves have an average lifespan of three years. Sleeves for 60" are typically priced around $155.00 (Aquafine, n.d.-a). Because quartz sleeves are replaced every three years, the cost can be distributed over these years. As such, assuming that 12 sleeves are needed once every three years, the annual cost

is $615.00 (Aquafine, n.d.-a). The quartz sleeves require cleaning every 12 months with a mild acid. The industry standard is CLR (ESP Water Products, n.d.). A minimal quantity will be needed for cleaning. To err on the side of caution, 4 gallons will be purchased annually. This comes out to be a cost of $108.00 per year (ULINE, n.d.). Energy costs to operate the unit are $1,393. In total, the cost to operate UV disinfection is $7,156.00 per year. This total cost was considered to be a utility cost in cash flow calculations.

The price of one kW-hour of energy was taken to be 6.09 rupee (Jaganmohan, 2020). With the power requirements already determined, the cost of powering the pumps in the design needed to be calculated. All pumps were assumed to have an efficiency of 75%, in accordance with calculations in the engineering economics textbook (Turton et al., 2016). The pumps used in RO are a special case in that the amount of power it takes to run them depends on the operating season. The costs of running RO pumps for each season and for the whole year can be seen in Table 11.2.2. It was calculated that backflushing would require 6.37 kW of power per stage to backflush permeate water through the membranes using the same equations above (only costs about $9,200 USD/year in total for Reverse Osmosis). Due to how low this cost is relative to the main costs of pumping for reverse osmosis, backflushing power costs were neglected in economic calculations for reverse osmosis. Power costs for microfiltration backflushing were also neglected (costing about $1290/year).

Table 11.2.2 Costs of running RO pumps.

	Pre-monsoon season	Post Monsoon season
kW to Sustain Operation	766.29	517.92
Days in Operating Season	181.00	184.00
kW hours for Operation Season	3,328,747.34	2,287,130.51
kW hours produced from HTL	1,307,222.22	1,328,888.89
Net Cost of Operation/Season	$160,044.14	$75,863.99
Net Annual Operating Cost	$235,908.13/year	
Amount Saved from HTL	$208,700.92/year	

The rest of the pumping power costs were determined year round because the mode of operation does not change with the season. The remaining costs of power can be seen in Table 11.2.3.

Table 11.2.3 Other pumping power costs.

Process	Pumping Power Required (kW)	Cost (USD/year)
Microfiltration Pump Power	62.53	$43,365.73
Sedimentation Pump Power	41.59	$28,843.88
HTL Pump Power	2,620.00	$75,710,271.00

Finally, the cost of the replacement reverse osmosis and microfiltration membranes need to be determined. Throughout the year, membranes will be replaced. At the end of each year, a new set of membranes will need to be bought to ensure a high flux of water without any membrane fouling or plugging. The cost of these membranes were estimated using the price of commercial RO membranes (FilterWater, n.d.). For microfiltration, the membrane price was

estimated using the price of a commercial hollow fiber membrane with a similar flux (MadeInChina, n.d.). The annual cost of microfiltration membranes was estimated to be $800/membrane. With 24 microfilter units, the annual cost of microfiltration membranes was estimated to be $19,200. The RO process consists of two types of membranes: brackish water membranes in Stage 1 and saltwater membranes in Stages 2 and 3. For Stage 1, the price of a brackish water membrane was estimated to be $780/membrane. For Stages 2 and 3, the price of a saltwater membrane was estimated to be $960/membrane. With 26 pressure vessels in Stage 1 and 21 pressure vessels in Stages 2 and 3 with 7 membranes in each pressure vessel, the total annual cost of RO membranes was estimated to be $283,080, bringing the total annual cost of microfiltration and RO membranes to $302,280. The cost of microfiltration filters and reverse osmosis membrane replacements were considered to be utility costs when performing economic analyses.

With all of these costs determined, the annual operating cost was determined using an equation from the engineering economics text (Turton et al., 2016):

$$COM_d = 0.180 * FCI + 2.73 * C_{OL} + 1.23 * (C_{UT} + C_{WT} + C_{RM}) \quad (11.2.2)$$

where COM_d is the cost of operation without depreciation, FCI is the fixed capital investment, C_{OL} is the cost of operating labor (and 2.73 accounts for any supervisors and managers needed), C_{UT} is the cost of utilities, and C_{RM} is the cost of raw materials. The C_{WT} term can be neglected since the design does not require any outside waste treatment. Plugging the cost of additional utilities needed in for C_{UT}, the cost of $Na_2S_2O_4$ in for C_{RM}, and the annual cost of operator wages in for C_{OL}, the only thing left to determine was the FCI. The sum of all of the capital costs

discussed in section 11.1 were multiplied by a Lang Factor of 4.61. This value was recommended by Capcost (Turton, 2017), and is very close to the recommended value for a fluids processing plant (Turton et al., 2016). This sum, the Total Capital Investment (TCI), is related to the FCI by equation 11.2.3:

$$TCI = FCI + WC \quad (11.2.3)$$

where WC is the working capital investment. Approximating the WC as 10% of the FCI, the FCI was calculated to be $239 million. With these values, the annual cost of operation without depreciation was determined to be approximately $162 million/year.

11.3 Revenue

With the production of 10,052 m^3/day (10,052,000 L/day) of water, the revenue can be estimated by assigning a price for the water produced. The price for private water suppliers in Chennai is 7.5 rupee/L according to one source (Rao, 2019), which equates to approximately $0.10/L. This gives an estimated revenue of about $1 million/day or $367 million/year.

11.4 Cash Flow, Return on Investment, and Internal Rate of Return

With the total cost of capital investment determined, the cashflow for all 20 years of operation was determined. During the first year of plant operation, it was assumed that only half of the production (and therefore half of the revenue) could be achieved as plant operations were finalized. All 20 years of plant operation assumed full, uninterrupted operation. Seven year straight line depreciation of assets was used to adjust taxes accordingly for the first seven years

of operation. This means that $\frac{1}{7}$ of the TCI was subtracted from the gross profit to calculate the amount of taxes owed. At the end of year 20, it was assumed that the recovery cost from selling the land and equipment used in the process equates to twice the amount that was invested as working capital. The internal rate of return turned out to be 38.62%, indicating a profitable investment. The parameters used in the cash flow analysis can be seen in Table 11.4.1, and the results of the analysis can be seen in Table 11.4.2.

Table 11.4.1 Cash flow parameters.

Parameter	Amount (million USD/year)
Total Capital Investment (TCI)	263.0
Fixed Capital Investment (FCI)	239.0
Working Capital (WC)	23.9
Seven Year Straight Line Depreciation Value	37.6
Annual Revenue	367.0
Annual Expenses	162.0

Table 11.4.2 Cash flow analysis.

Year	-2	-1	0	1→7	8→19	20
Investment (million USD)	-120	-120	-23.9	-	-	47.9
Notes	Land, Equip, Construction	Equip, Construct	WC	-	-	WC, land, salvaging
Revenue (million USD)	-	-	183.0	367.0	367.0	367.0
Expenses (million USD)	-	-	162.0	162.0	162.0	162.0
Gross Profit (million USD)	-	-	0.0	205.0	205.0	205.0
Taxes (million USD)	-	-	0.0	50.3	61.6	76.0
After-tax Cash flow (million USD)	-120	-120	-2.04	155.0	144.0	177.0

11.5 Alternate Scenarios

1. HTL is not traditional to wastewater treatment plants, so an alternate scenario in which HTL is not run was also considered. This scenario eliminates the cost of HTL operations and any associated capital costs in a second cash flow analysis. As a result, all power required for the process was supplied by utility power, and labor required for HTL was not taken into account. Additionally, the cost to landfill the sewage removed by sedimentation was taken to be 70,000 rupees/month, which converts to $10,920 USD/year (The New Indian Express, 2022). The results can be seen in Table 11.5.1. The most noteworthy difference between the proposed and alternate scenarios is the value of the after-tax cash flows in year 0. This after-tax cash flow is significantly greater in the alternate scenario compared to the actual scenario (a 4802% increase), which makes sense due to the great cost of operating HTL (pumps, equipment, and operators). The after tax flows for every other year only show a percent increase between 37.6% to 47.3% due to the increase in taxes in the alternate scenario. This also results in an IRR value of 58.90%. Overall, running this alternate scenario demonstrates that while HTL operation may decrease profits for the plant, the cost to do so does not become hugely significant in later years (as the plant still profits). Processing the biowaste into something useful rather than just dumping it into the ocean or into a landfill doesn't cost significantly more (at least not to the point that the plant operation isn’t economically feasible). This is good for the environment without costing too much, as the plant will still profit either way. Therefore, maintaining the HTL reaction is still recommended from both an economic and environmental perspective.

2. HTL is a novel reaction that has many benefits to the environment and is therefore an exciting new prospective process. However, because HTL is still so novel, many of the details of the reaction are unknown. As a result, the large-scale process design likely has many areas of improvement. Another scenario that might improve upon the design outlined in this report is a continuous upstream HTL process. The downstream process, or the power cycle, is continuous, and the boiler is constantly running and the turbine is constantly producing electricity. When the HTL reactor is operating, the steam from the turbine is compressed and flows into the reactor for heating, which is a relatively efficient use of the steam. When the HTL reactor is not operating, however, the hot steam leaving the turbine is immediately condensed to be recycled back through the boiler. This condensing is a significant energy drain and decreases the efficiency of this process. To design a continuous upstream process, multiple HTL reactors would be installed and one reactor would be running at all times. This would provide a constant use for the steam from the turbine, which would eliminate the condenser and recycle stream to the boiler, increasing the efficiency of the power cycle. A design of this scale is entirely possible with the amount of raw sewage available, and would produce significantly more bio-crude oil and char on a daily basis, increasing profit, although a larger capital investment is required. Another benefit to creating a continuous process is the safety aspects. A continuous process is always more safe than a batch system because of the inherent hazards that arise from starting up and shutting down process elements.

Table 11.5.1 Alternate cash flow analysis.

Year	-2	-1	0	1→7	8→19	20
Investment (million USD)	-115	-115	-23.0	-	-	46.0
Notes	Land, Equip, Construction	Equip, Construct	WC	-	-	WC, land, salvaging
Revenue (million USD)	-	-	183.0	367.0	367.0	367.0
Expenses (million USD)	-	-	64.4	64.4	64.4	64.4
Gross Profit (million USD)	-	-	0.0	302.0	302.0	302.0
Taxes (million USD)	-	-	0.0	79.9	90.7	105.0
After-tax Cash flow (million USD)	-115	-115	96.0	222.6	211.7	244.0

11.6 Distribution of Water

The increased awareness of the importance of clean water for maintaining good health is creating a growing demand for bottled water in India. Additionally, many tourists prefer bottled water instead of tap water, providing another incentive to bottle water in India. Therefore, the water will be distributed to residents by first sending the finished product to a bottling facility, which will then distribute the bottled water directly to residents who need it the most. It is important that the water be distributed to rural areas, as bottled water is significantly less distributed in these areas (Netscribes (India) Pvt. Ltd, 2019). The bottling plant/company will most likely want to set the bottled water at a significantly higher price than the purchasing price of the water itself, and the price of the water for this design plant was modified accordingly to ensure that the bottled water could be affordable. In order to avoid a significant upcharge in the price of the bottled water, any potential contracts with a bottling company will include pricing limits. Most bottled water in India sells for at least ₹20 per liter, though several brands cost upwards of ₹100 per liter (BigBasket, 2022). Though the exact retail pricing is outside the scope of this project, it would be less than ₹20 per liter. All cash flow and other economic analyses performed assume that revenue only comes from selling the water to a bottling plant. In other words, the bottling plant does not return a percentage of sales back to the water treatment facility. This tradeoff has been made in an effort to encourage adherence with the imposed price-caps.

12. Safety, Health, Environment, and Social Impacts

12.1 Material Compatibility

As the design involves mostly filtration and separation processes, there is only one hazardous chemical being used. The cleaning solution for the reverse osmosis membranes and microfiltration filters, sodium dithionite, is flammable and is an irritant. According to safety data information, the chemical may ignite when exposed to moisture and reacts vigorously in contact with water. The chemical is also a potential irritant for the skin, eyes, and respiratory system. Both of these hazards are concerning since the chemical is mixed with water in a storage tank on site to make the cleaning solution (National Center for Biotechnology Information, 2022).

12.2 Credible Events and Mitigations

Credible events/incidents that are most likely to occur are loss of containment from tanks and vessels. These can be caused by overfilling vessels or leaks in process equipment. Another main area of safety concern is pump and compressor seal failures, which is especially important given the high number of pipes present in the design. Rupture within the pipes themselves is another area of concern.

12.2.1 Loss of Primary Containment (LOPC)

The main concern of this design is that large quantities of hazardous materials are being stored and transported. In addition to the hazardous cleaning solution, the other dangerous materials are hazardous biomass being collected for HTL and the oil, char, and gases (mainly CO_2) that are produced from it. The char and oil are fed into a common storage tank and agitated

before being taken to the boiler to be burned. Therefore, a loss of containment in any storage vessel due to a leak in it could cause the release of flammable or ignitable materials. The loss of containment in the sedimentation tanks can result in the release of the wet biomass collected from the river.

In order to mitigate these potential losses of containment, several implementations will be made. Dikes surrounding storage vessels are a basic mitigation to contain any spills. Additionally, the char and oil storage tank and the sodium dithionite storage tanks should be stored far from other equipment in the process should accidental ignition occur to limit the effects of one. A high level sensor will be implemented into all storage tanks (for sedimentation, HTL products, and cleaning solution) to alert operators when overflow occurs (Crowl and Louvar, 2019). All operators working near or with these storage tanks will be required to wear full personal protective equipment (PPE). According to the National Center for Emerging and Zoonotic Infectious Diseases (NCEZID), the recommended PPE for drinking water treatment plant operators includes goggles, a splash proof face mask or shield, liquid-repellant full body coveralls, waterproof gloves, and rubber boots (2021).

12.2.2 Pump and Compressor Failures and Pipe Ruptures

The failure of the pumps, pipes, or the compressor could result in the dire incidents in the process. The spillage of dirty water, biohazards, crude oil, or cleaning solution during process operation could expose operators to biohazards and/or skin irritants. Compressor failures could cause the release of superheated steam, which can cause skin burns to operators. Basic mitigations to address these issues start with secondary pumps and a secondary compressor put in place (and accounted for in the capital costs) to provide a safe route for flow should the original equipment fail. Drains, seals, pumps, and pipes should be regularly inspected and tested

by operators. It is recommended that the equipment be inspected then replaced/repaired if needed once every year on the first Monday in February (U.S. Environmental Protection Agency, n.d.).

Safeguards that will be implemented include pressure sensors in every pump that sends an alert to an operator when the pressure drops too low (indicating a leak). This alert would also activate a central interlock system that would shutdown all pumps in the process should a leak occur. All of the pipes, the pumps, and the compressor in the design will be equipped with flowmeters that monitor flow. If the flow drops below normal operating levels, the central interlock system will then be activated to shut off the pumps in the process.

12.3 Environmental Impacts of Plant

The environmental impact of the plant is dependent on the waste streams and byproducts of the process. These waste streams include highly concentrated wastewater from reverse osmosis, the sodium dithionite cleaning solution waste, and carbon dioxide from HTL. First, the waste from reverse osmosis should not have any significant environmental impact. The stream will be pumped into the Bay of Bengal. The average TDS concentration of the waste stream is 29,110 mg/L, and the average TDS concentration in the Bay of Bengal is 27,140 mg/L (Rashid et al., 2013). This difference in concentration is not significant enough to cause any sort of change to concentration of the Bay of Bengal or affect the ecosystem at the discharge site.

The cleaning solution for reverse osmosis and microfiltration is considered hazardous waste. It is extremely bad for aquatic environments and can negatively affect plant growth and wildlife health if exposed at high enough concentrations. The 1.0% (W) sodium dithionite solution used in the process is at low concentrations for this reason. There are also specific steps taken to ensure the cleaning solution never reaches the reverse osmosis waste stream. The

cleaning solution is held in a storage tank separate from the RO and microfiltration systems. When cleaning the membranes, the cleaning solution is cycled back to the storage tank never entering the RO waste stream. When disposing of the cleaning solution, the plant will follow the protocols made by the Department of Environmental Protection (DEP) and will dispose of the contents at an approved waste disposal plant to ensure proper and environmentally safe disposal of the sodium dithionite solution.

The HTL gas stream is mainly composed of CO_2, but also holds significant amounts of CO and CH_4. Treatment was considered for this flue gas due to the increasing concentration of greenhouse gases in the atmosphere. Due to economic and scope considerations, treatment was ruled out. The two main options of stripping columns and sequestration both prove to be quite expensive in implementation due to an increase in capital costs as well as raw material costs (such as the costs of compounds like amines required in the stripper). The CO and CH_4 do pose serious risk though, so treatment of the flue gas must be considered for future consideration.

12.4 Social Impacts of Plant

The Cooum River was once seen as a sacred river that local residents would swim in to achieve salvation and prior to prayers when it was clean enough to do so (Jishamoli, 2018). Fishing was also a popular river activity for residents, but now fish can only survive in the water for just a few hours before succumbing to the pollutants. By implementing many drinking water treatment plants (from this design) along the river that make use of the sewage rather than dumping it into the ocean, the river could eventually become clean enough to the point that residents can resume activities that they once used to enjoy. However, HTL would need to be scaled up accordingly to accommodate the sewage that comes from industries, retail outlets,

corporations, and family homes that line the river and dump sewage into it (Jishamoli, 2018). At the end of the day, there is a possibility that the biomass processing aspect of the design will help restore the holy status that the river once had.

Another notable impact is that residents will be less stressed knowing that they have more access to clean water. Aside from the river itself being contaminated, climate change has created increasingly unreliable rains during the monsoon season. As this is the city's only source of unpolluted drinking water, this instability creates a humanitarian crisis. Current water distributors charge a surplus for clean bottled water. This creates a vast divide between those who can afford to drink clean water, remain healthy, and stay safe, and those who can not. By providing potable water at a lower cost, the project will begin to bridge that divide. Additionally, entering the market with a lower cost product may encourage competitors to lower their prices, establishing a more equitable environment regarding water access in Chennai.

13. Conclusions and Recommendations

The design of the Chennai water treatment plant required many assumptions due to availability of public data regarding the contents of the river and hydrothermal liquefaction. If this project were to be developed, a fully updated characterization of the river and its contents would be required. The composition of the river is variable and should be considered for any changes in balances and operating conditions. The same uncertainty is present when considering the hydrothermal liquefaction process design. There has been no research involving larger scale HTL reactions, so to ensure a successful design, more in depth understanding of the kinetics and mechanics of HTL reactions would be required.

Through this design, HTL has been shown to be an interesting and practical process for power generation with an organic feedstock. The plant shows overall profit for almost every year when HTL is included in the design, not including the significant environmental benefits of HTL to the Cooum river and surrounding environment. With an IRR of 38.62%, the investment in HTL shows promise through economic analysis. Therefore, the design team recommends that both HTL and the drinking water treatment aspects of the plant be implemented.

14. Acknowledgements

The design team would like to thank Professor Eric Anderson for his dedication and motivation to help answer any overall design questions and for providing feedback during project checkpoints. Professor Lisa Colosi Peterson, associate professor in the Department of Engineering Systems & Environment, served as a very helpful source when gaining information about the relatively novel process of hydrothermal liquefaction, and her research in the field was most valuable when learning how to implement the reaction into the design. Professor Aaron L. Mills, professor in the Department of Environmental Sciences, provided knowledge of traditional water treatment processes and aided the team in sedimentation tank and UV disinfection design. Professor Geoffrey M. Geise, associate professor in the Department of Chemical Engineering, provided knowledge and helpful resources for the design of the reverse osmosis and microfiltration systems. Professor Ron J. Unnerstall, Professor of Practice - Chemical Process Safety, provided guidance in the hazard, safety, and mitigations analysis of the design. The team would like to extend gratitude and a big thank you to all of these valuable mentors.

15. Works Cited

Abinandan, S., Aravind, U., Ganapathy, G. P., & Shanthakumar, S. (2019). Distribution of Metal Contamination and Risk Indices Assessment of Surface Sediments from Cooum River, Chennai, India. *International Journal of Environmental Research*, *13*(5), 853–860. https://doi.org/10.1007/s41742-019-00222-8.

Agoramoorthy, G. (2014). Sacred Rivers: Their Spiritual Significance in Hindu Religion. Journal of Religion and Health, 54(3), 1080–1090. https://doi.org/10.1007/s10943-014-9934-z.

Anirudhan, I. V., & Ramaswamy, S. V. (2009). Experience with expansive soils and shales in and around Chennai. IGC. Retrieved January 10, 2022, from https://gndec.ac.in/~igs/ldh/conf/2009/articles/V2-0_07.pdf

Aquafine. (n.d.-a). Aquafine 18348, 60" Quartz Sleeve, Double Ended. Serv A Pure. Retrieved April 1, 2022, from https://www.servapure.com/Aquafine-18348-60-Quartz-Sleeve-Double-Ended_p_2599.html

Aquafine. (n.d.-b). Aquafine, 60" UV Lamp, GOLD-L, Disinfection Lamp. Serv A Pure. Retrieved April 1, 2022, from https://www.servapure.com/Aquafine-60-UV-Lamp-GOLD-L-Disinfection-Lamp_p_2583.html

AWC. (n.d.). Reverse osmosis chemicals: membrane cleaning chemicals. American Water Chemicals, Inc. Retrieved February 14, 2022, from https://www.membranechemicals.com/product-category/ro-chemicals-ronf/

Bagajewicz, M. J., Savelski, M. J. (2013). *Flash Drum Design* [PowerPoint Slides]. https://www.ou.edu/class/che-design/design%201-2013/Flash%20Design.pdf

Basu, O. D. (2015). Backwashing. *Encyclopedia of Membranes, Springer Berlin Heidelberg, Berlin, Heidelberg*, 1-3.

Bhattacharya, P., Roy, A., Sarkar, S., Ghosh, S., Majumdar, S., Chakraborty, S., Mandal, S., Mukhopadhyay, A., & Bandyopadhyay, S. (2013). Combination technology of ceramic microfiltration and reverse osmosis for tannery wastewater recovery. *Water Resources and Industry*, *3*, 48–62. https://doi.org/10.1016/j.wri.2013.09.002.

Bhavan, M. (2012, May). *Indian Standard Drinking Water — Specification (Second Revision)*. Retrieved November 17, 2021, from http://cgwb.gov.in/Documents/WQ-standards.pdf.

BigBasket. (2022). Mineral Water. bigbasket. Retrieved April 10, 2022, from https://www.bigbasket.com/pd/197351/bisleri-mineral-water-1-l-carton/

British Columbia Ministry of Environment. (2016, July). A User Guide for Assessing the Design, Size, and Operation of Sediment Ponds Used in Mining.

Bullard, F. & Salas, J. (n.d.). Industrial UV sterilizers UVI. Pure Aqua. Inc. Retrieved April 2, 2022, from https://pureaqua.com/industrial-uv-sterilizers/

Castello, D., Pedersen, T. H., & Rosendahl, L. A. (2018). Continuous hydrothermal liquefaction of biomass: A critical review. *Energies*, *11*(11), 3165.

Central Pollution Control Board, Ministry of Environment and Forests. (n.d.). *Status of Water Treatment Plants in India*. Retrieved April 8, 2022, from https://cpcb.nic.in/openpdffile.php?id=UmVwb3J0RmlsZXMvTmV3SXRlbV8xMDNfc3RhdHVzb2Z3YXRlcnF1YWxpdHlwYWNrYWdlLnBkZg==.

Cheng, F., Porter, M. D., & Colosi, L. M. (2020). Is hydrothermal treatment coupled with carbon capture and storage an energy-producing negative emissions technology? *Energy Conversion and Management*, *203*. https://doi.org/10.1016/j.enconman.2019.112252.

Chennai Population. World Population. (2021). Retrieved November 18, 2021, from https://www.populationu.com/cities/chennai-population.

Chennai Rivers Restoration Trust. (2020). *Cooum River - CRZ Compliance Report*. Retrieved February 17, 2022, from http://www.chennairivers.gov.in/CRRestoration.html.

Corrosionpedia. (2019, April 20). *What Does Total Dissolved Solids (TDS) Mean?* Retrieved February 13, 2022, from https://www.corrosionpedia.com/definition/1103/total-dissolved-solids-tds.

Crocker, M. (Ed.). (2010). Thermochemical conversion of biomass to liquid fuels and chemicals. Royal Society of Chemistry.

Crowl, D. A., & Louvar, J. F. (2019). Chapter 5. Hazardous Material Dispersion. In *Chemical Process Safety: Fundamentals with Applications* (4th ed., pp. 177–218). essay, Pearson.

Daal, L., Vos, F. de, Soons, J., & Vries, T. de. (2015). Spiral-Wound Module. Retrieved February 11, 2022, from https://www.sciencedirect.com/topics/engineering/spiral-wound-module.
Figure 20.9.

Dammel, E. E., & Schroeder, E. D. (1991). Density of activated sludge solids. Water research, 25(7), 841-846.

Darestani, M. T., Chilcott, T. C., & Coster, H. G. (2014). Effect of poling time on filtration properties of PVDF membranes treated in intense electric fields. *Polymer Bulletin*, *71*(4), 951–964. https://doi.org/10.1007/s00289-014-1103-8.

Dhamodharan, A., Ganapathy, G. P., & Shanthakumar, S. (2016). Assessment of seasonal variations in surface water quality of Cooum River in Chennai, India – a statistical approach. Issue 3, 18(3), 527–545. https://doi.org/10.30955/gnj.001787

Dupont. (2020a). *FilmTec™ SW30HRLE-400 Element*. Product Data Sheet. Retrieved February 14, 2022, from https://www.dupont.com/content/dam/dupont/amer/us/en/water-solutions/public/documents/en/45-D00967-en.pdf.

Dupont. (2020b). *FilmTec™ BW30-400 Membranes*. Product Data Sheet. Retrieved February 14, 2022, from https://www.dupont.com/content/dam/dupont/amer/us/en/water-solutions/public/documents/en/45-D01505-en.pdf.

DuPont. (2022, February). *Cleaning Procedures for FilmTec™ FT30 Elements*. Product Data Sheet. Retrieved February 14, 2022, from https://www.dupont.com/content/dam/dupont/amer/us/en/water-solutions/public/documents/en/RO-NF-FilmTec-Cleaning-Procedures-Manual-Exc-45-D01696-en.pdf.

Eichhorn, S., S., H. J. W., Jaffe, M., & Demeuse, M. T. (2009). 15 - Production and applications of hollow fibers. In *Handbook of Textile Fibre Structure* (Vol. 2, pp. 485–499). essay, Woodhead Pub. Retrieved November 17, 2021, from https://www.sciencedirect.com/science/article/pii/B9781845697303500159.

Elangovan, N. S., & Dharmendirakumar, M. (2013, March 11). Assessment of groundwater quality along the Cooum River, Chennai, Tamil Nadu, India. Journal of Chemistry. Retrieved November 18, 2021, from https://www.hindawi.com/journals/jchem/2013/672372/.

Elliott, D. C., Biller, P., Ross, A. B., Schmidt, A. J., & Jones, S. B. (2015). Hydrothermal liquefaction of biomass: Developments from batch to continuous process. *Bioresource technology*, *178*, 147-156.

ESP Water Products. (n.d.). Learn about UV water purification: ESP water products. ESPWaterProducts.com. Retrieved March 18, 2022, from https://www.espwaterproducts.com/understanding-uv-water-filtration-sterilization/#:~:text=During%20the%20UV%20water%20disinfection,ability%20to%20function%20and%20reproduce.

Express News Service. (2020, March 18). *Industries being provided water at Rs 27.54 per 1,000 litres: Gujarat govt to Assembly*. The Indian Express. Retrieved April 2, 2022, from https://indianexpress.com/article/india/industries-being-provided-water-at-rs-27-54-per-1000-litres-gujarat-govt-to-assembly-6320907/.

Feher, J. (2017). Osmotic Coefficient. Retrieved February 13, 2022, from https://www.sciencedirect.com/topics/engineering/osmotic-coefficient.

FilterWater. *Commercial reverse osmosis membranes*. FilterWater.com - Water Filters and Filtration Systems. (n.d.). Retrieved April 10, 2022, from https://www.filterwater.com/c-37-commercial-membranes.aspx?gclid=cj0kcqjwgmqsbhdcarisaiivn1ui7nft_s0zw4b4an0ay-f3ksh_9ggg9achkd5elpjwzycn7ks6bd0aahzcealw_wcb

Final Screening and Grit Removal - US EPA. (n.d.). Retrieved March 5, 2022, from https://www3.epa.gov/npdes/pubs/final_sgrit_removal.pdf

Flottweg Separation Technology. (2016). *The New Flottweg Decanter Z3E*. Vilsbiburg, Germany; Flottweg SE. Retrieved February 28, 2022, from https://www.flottweg.com/fileadmin/user_upload/data/pdf-downloads/Z3E_EN.pdf.

Fravel, H. (2014, April 28). *Understanding The Critical Relationship Between Reverse Osmosis Recovery Rates and Concentration Factors*. Retrieved February 13, 2022, from https://www.wateronline.com/doc/understanding-the-critical-relationship-between-reverse-osmosis-recovery-rates-and-concentration-factors-0001.

Furtado, R. (2019, October 21). Laws existing in India to prevent and Control Water Pollution. iPleaders. Retrieved March 4, 2022, from https://blog.ipleaders.in/laws-existing-india-prevent-control-water-pollution/

Ganapathy, V. S., Radhakrishnan, K., & Prakasheswar, P. (2021). A baseline study on the occurrence and distribution of microplastics in the highly polluted Metropolitan River Cooum, Chennai, India. Environmental Science and Pollution Research. https://doi.org/10.21203/rs.3.rs-720731/v1

Giridharan, L., Venugopal, T., & Jayaprakash, M. (2009). Assessment of water quality using chemometric tools: A case study of river cooum, South India. *Archives of Environmental Contamination and Toxicology*, *56*(4), 654–669. https://doi.org/10.1007/s00244-009-9310-2.

Godsey, W. E. (n.d.). *Fresh, Brackish, or Saline Water for Hydraulic Fracs: What are the Options?* Retrieved February 14, 2022, from https://www.epa.gov/sites/default/files/documents/02_Godsey_-_Source_Options_508.pdf.

Gollakota, A. R. K., Kishore, N., & Gu, S. (2018). A review on hydrothermal liquefaction of biomass. *Renewable and Sustainable Energy Reviews*, 81, 1378–1392. https://doi.org/10.1016/j.rser.2017.05.178.

Gopal, K., Tripathy, S. S., Bersillon, J. L., & Dubey, S. P. (2007). Chlorination byproducts, their toxicodynamics and removal from drinking water. Journal of hazardous materials, 140(1-2), 1–6. https://doi.org/10.1016/j.jhazmat.2006.10.063

Gowri, V. S., Ramachandran, S., Ramesh, R., Pramiladevi, I. R., & Krishnaveni, K. (2007). Application of GIS in the study of mass transport of pollutants by Adyar and Cooum Rivers in Chennai, Tamilnadu. *Environmental Monitoring and Assessment*, *138*(1-3), 41–49. https://doi.org/10.1007/s10661-007-9789-9.

Gregory, R., & Bache, D. H. (2021). Sedimentation Processes. IWA Publications. Retrieved April 10, 2022, from https://www.iwapublishing.com/news/sedimentation-processes

Gulliver, J. S., & Holzaski, R. M. (2010). Sedimentation Practices. Stormwater Treatment: Assessment and Maintenance. Retrieved March 8, 2022, from http://stormwaterbook.safl.umn.edu/sedimentation-practices#:~:text=Using%20Stokes%27%20Law%2C%20the%20settling,C%20(90%20%C2%B0F).

Gupta, R. K., Dunderdale, G. J., England, M. W., & Hozumi, A. (2017). Oil/Water Separation Techniques: A review of recent progresses and Future Directions. *Journal of Materials Chemistry A, 5*(31), 16025–16058. https://doi.org/10.1039/c7ta02070h.

Halpert, M. S., & Bell, G. D. (n.d.). *Indian summer monsoon*. Climate Assessment for 1996. Retrieved April 2, 2022, from https://www.cpc.ncep.noaa.gov/products/assessments/assess_96/india.html.

Hancock, N. (2018, August 15). *Ultrafiltration, Nanofiltration, and Reverse Osmosis*. Retrieved November 24, 2021, from https://www.safewater.org/fact-sheets-1/2017/1/23/ultrafiltrationnanoandro.

Huber. (2022, March 8). Huber Multi-Rake Bar Screen RakeMax®. Huber Technology Inc. Retrieved May 1, 2022, from https://www.huber-technology.com/products/screens-and-fine-screens/perforated-plate-and-bar-screens/huber-multi-rake-bar-screen-rakemaxr.html

Huehmer, R., Gomez, J., Curl, J., & Moore, K. (2011). *Cost modeling of desalination systems*. Retrieved April 11, 2022, from https://www.researchgate.net/profile/Robert-Huehmer/publication/299408931_COST_MODELING_OF_DESALINATION_SYSTEMS/links/56f458fa08ae81582bf0a346/COST-MODELING-OF-DESALINATION-SYSTEMS.pdf

IHI. (2022). IHI centrifuge: TP: Screw decanter centrifuge: Separator,dehydrator. Retrieved March 25, 2022, from https://www.ihi.co.jp/separator/en/products/screw/tp.html

Indeed. (2022, March 7). *Operations Engineer salary in India*. Job Search India. Retrieved April 2, 2022, from https://in.indeed.com/career/operations-engineer/salaries.

Jaganmohan, M. (2020, November 16). *India - Cost of State Electricity Supply*. Statista. Retrieved November 19, 2021, from https://www.statista.com/statistics/808201/india-cost-of-state-electricity-supply/.

Jishamoli, B. (2018, September). *The Water Resources in Chennai: Cooum River*. Retrieved April 10, 2022, from https://www.researchgate.net/profile/Jishamol-B/publication/339041197_The_water_resources_in_Chennai_Cooum_River/links/5e3a31d892851c7f7f1d02d8/The-water-resources-in-Chennai-Cooum-River.pdf.

Kohl, H., Bennett, I., Schmitt, T., Virden, J., & Anderson, N. (2019). Industrial Effluent to Potable Drinking Water Along Lerma River with Energy Recovery. *Undergraduate Thesis Portfolio*, 25–66.

Krishnamurthy, R., & Desouza, K. C. (2015). Chennai, India. *Cities*, *42*, 118–129. https://doi.org/10.1016/j.cities.2014.09.004.

Li, M. (2012). Optimal plant operation of brackish water reverse osmosis (BWRO) desalination. *Desalination*, *293*, 61–68. https://doi.org/10.1016/j.desal.2012.02.024.

Lu, Y.-Y., Hu, Y.-D., Zhang, X.-L., Wu, L.-Y., & Liu, Q.-Z. (2007). Optimum design of reverse osmosis system under different feed concentration and product specification. *Journal of Membrane Science*, *287*(2), 219–229. https://doi.org/10.1016/j.memsci.2006.10.037.

MadeInChina. *Hollow fiber ultrafiltration membrane for UF water filter cartridge*. MadeInChina. (n.d.). Retrieved April 10, 2022, from https://jinhuimouf.en.made-in-china.com/product/hBrEYinVvFUt/China-Hollow-Fiber-Ultrafiltration-Membrane-for-UF-Water-Filter-Cartridge.html

MBR Screening Part 2: Selecting an MBR screen. The MBR Site. (n.d.). Retrieved March 4, 2022, from https://www.thembrsite.com/features/membrane-bioreactor-screening-part-2-selecting-an-mbr-screen/

MECC. (n.d.). Sedimentation. MECC. Retrieved February 10, 2022, from https://water.mecc.edu/courses/ENV115/lesson6.htm

Minnesota Rural Water Association. (n.d.). Sedimentation - MRWA. Minnesota Rural Water Association. Retrieved February 10, 2022, from https://www.mrwa.com/WaterWorksMnl/Chapter%2013%20Sedmentation.pdf

Murphy, S. (2007, April 23). *Basin: General Information on Solids*. Retrieved February 26, 2022, from http://bcn.boulder.co.us/basin/data/NEW/info/TSS.html.

National Center for Biotechnology Information (2022). PubChem Compound Summary for CID 24489, Sodium dithionite. Retrieved April 8, 2022 from https://pubchem.ncbi.nlm.nih.gov/compound/Sodium-dithionite.

National Center for Emerging and Zoonotic Infectious Diseases (NCEZID). (2021, December 9). *Guidance for Reducing Health Risks to Workers Handling Human Waste or Sewage*. Centers for Disease Control and Prevention. Retrieved April 7, 2022, from https://www.cdc.gov/healthywater/global/sanitation/workers_handlingwaste.html#:~:text=Goggles%3A%20to%20protect%20eyes%20from,to%20human%20waste%20or%20sewage.

Netscribes (India) Pvt. Ltd. (2019, March 1). *Bottled Water Market in India (2018-2023)*. Market Research. Retrieved April 10, 2022, from https://www.marketresearch.com/Netscribes-

India-Pvt-Ltd-v3676/Bottled-Water-India-12269919/#:~:text=The%20major%20bottled%20water%20brands,barrels%20of%2015%2D20%20liters.

Outback Water. (n.d.). Instructions On How To Clean and Replace The UV Quartz Sleeve For OutbackWaterTM and other LuminorTM Manufactured UV Systems.

Ovsyannikova, E., Kruse, A., & Becker, G. C. (2021). Valorization of Byproducts from Hydrothermal Liquefaction of Sewage Sludge and Manure: the Development of a Struvite-Producing Unit for Nutrient Recovery. *Energy & Fuels*, *35*(11), 9408-9423.

Pall Water. (2022-a). *Microza Hollow Fiber Una Modules*. Ultrapure Water. Retrieved February 26, 2022, from https://shop.pall.com/us/en/microelectronics/semiconductor/ultrapure-water-1/zidgri78l6l

Pall Water. (2022-b). *Water Filtration Modules and Membranes*. Retrieved February 26, 2022, from https://www.pallwater.com/products/modules-and-membranes?_bk=pall+membrane+filters&_bm=b&_bt=391186752659&_bn=g&_bg=79352344468&utm_id=go_cmp-1953587491_adg-79352344468_ad-391186752659_kwd-301480882708_dev-c_ext-_prd-&utm_source=google&gclid=CjwKCAiAvOeQBhBkEiwAxutUVH8tWbpQCIkEQ9sO-O_lrOGlmiiUHBvrnjzeDYcD8UHhlOXIrXTSKxoCLnkQAvD_BwE.

Pall Corporation. (2022). *AquaSep® Plus L/L Coalescer*. Retrieved February 28, 2022, from https://shop.pall.com/us/en/products/coalescers/liquid-liquid/aquasep/aquasep-plus

Perry's Chemical engineers' handbook. (1984). New York :McGraw-Hill,

Peters, M. S., Timmerhaus, K. D., & West, R. E. (2002). *Plant design and economics for chemical engineers* (5th ed.). McGraw-Hill Professional.

Pureflow Inc. (2018, January 11). *Basics of Ultrafiltration*. Retrieved February 26, 2022, from https://www.pureflowinc.com/ultrafiltration/.

Puretec. (n.d.-a). *Basics of Reverse Osmosis - puretecwater.com*. Retrieved November 19, 2021, from https://puretecwater.com/downloads/basics-of-reverse-osmosis.pdf.

Puretec. (n.d.-b). *What is Reverse Osmosis? - puretecwater.com.* Retrieved February 14, 2022, from https://puretecwater.com/reverse-osmosis/what-is-reverse-osmosis.

Ramakrishnan, D. H., & Lakshmi, K. (2019, January 28). A mountain of trash fished out of Cooum. Retrieved February 13, 2022, from https://www.thehindu.com/news/cities/chennai/a-mountain-of-trash-fished-out-of-cooum/article26115438.ece

Raman, A. R. (2019, December 28). NDRF Clears 1 tonne waste from Cooum River: Chennai News. The Times of India. Retrieved April 10, 2022, from https://timesofindia.indiatimes.com/city/chennai/ndrf-clears-1-tonne-waste-from-cooum-river/articleshow/73004958.cms

Ramirez, J. A., Brown, R. J., & Rainey, T. J. (2015). A Review of Hydrothermal Liquefaction Bio-Crude Properties and Prospects for Upgrading to Transportation Fuels. *Energies*, *8*(7), 6765–6794. https://doi.org/10.3390/en8076765.

Rao, M. (2019, June 18). *Chennai water crisis: Private tankers fleece public, rates increase by over 100%*. The News Minute. https://www.thenewsminute.com/article/chennai-water-crisis-private-tankers-fleece-public-rates-increase-over-100-103859.

Raptor® Falconrake® Bar screen. Lakeside Equipment Corporation. (2020, May 7). Retrieved March 4, 2022, from https://www.lakeside-equipment.com/product/rake-bar-screen/

Rashid et al., 2:3 open access scientific reports. (n.d.). Retrieved March 5, 2022, from https://www.omicsonline.org/scientific-reports/2157-7617-SR-699.pdf

Riazi, A., Vila-Concejo, A., Salles, T., & Türker, U. (2020). Improved drag coefficient and settling velocity for carbonate sands. Scientific Reports, 10(1). https://doi.org/10.1038/s41598-020-65741-3

Rosendahl, L., Chen, W.-T., & Zhang , Y. (2018). 5 - Hydrothermal liquefaction of protein-containing feedstocks. In *Direct Thermochemical Liquefaction for Energy Applications* (pp. 127–168). essay, Elsevier Woodhead Publishing. Retrieved November 17, 2021, from https://www.sciencedirect.com/science/article/pii/B9780081010297000047.

Scholz, M. (2015). Wetland systems to control urban runoff. Elsevier Science & Technology.

ScienceDirect. (2015). Reverse Osmosis Membrane. Retrieved February 12, 2022, from https://www.sciencedirect.com/topics/engineering/reverse-osmosis-membrane.
Section: Membrane technologies for seawater desalination and brackish water treatment.

Semiat, R. (2010). *Reverse Osmosis Membrane*. Reverse Osmosis Membrane - an overview | ScienceDirect Topics. Retrieved March 4, 2022, from https://www.sciencedirect.com/topics/engineering/reverse-osmosis-membrane#:~:text=Operating%20pressures%20vary%20between%2010,and%2080%20bar%20for%20seawater.
Section: Water Purification: Materials and Technologies.

Smith, R. (1967). Compilation of cost information for conventional and advanced wastewater treatment plants and processes. US Department of the Interior.

Snowden-Swan, L. J., Zhu, Y., Jones, S. B., Elliott, D. C., Schmidt, A. J., Hallen, R. T., Billing, J. M., Hart, T. R., Fox, S. P., & Maupin, G. D. (2016). Hydrothermal Liquefaction and Upgrading of Municipal Wastewater Treatment Plant Sludge: A Preliminary Techno-Economic Analysis (PNNL--25464, 1258731; p. PNNL--25464, 1258731). https://doi.org/10.2172/1258731

Srinivasan. (2017). *Sewage lorries polluting Chennai lakes, drains with impunity.* Citizen Matters. Retrieved February 16, 2022, from https://chennai.citizenmatters.in/sewage-water-lorries-pollute-chennai-lakes-stormwater-drains-with-impunity-2096.

Swamee, P. K., & Tyagi, A. (1996). Design of class-I sedimentation tanks. Journal of Environmental Engineering, 122(1), 71–73. https://doi.org/10.1061/(asce)0733-9372(1996)122:1(71)

Texas Water Development Board. Seawater FAQ - Innovative Water Technologies | Texas Water Development Board. (n.d.). Retrieved March 4, 2022, from https://www.twdb.texas.gov/innovativewater/desal/faqseawater.asp#:~:text=Seawater%20typically%20is%20very%20salty,%3E35%2C000%20mg%2Fl.

The New Indian Express. (2022, March 15). *Firms engaged to handle waste, dump Chennai due to lack of cooperation*. Retrieved April 28, 2022, from https://www.newindianexpress.com/cities/chennai/2022/mar/15/firms-engaged-to-handle-wastedump-chennai-due-to-lack-of-cooperation-2430175.html.

TOI. (2019, November 20). *Chennai: 30 percent water samples fail quality test: Chennai News - Times of India*. The Times of India. Retrieved November 20, 2021, from https://timesofindia.indiatimes.com/city/chennai/30-water-samples-fail-quality-test/articleshow/72132907.cms.

Turton, R. (2017). *Richard Turton: Analysis Synthesis and Design of Chemical Processes 5th Edition*. Capcost 2017. Retrieved April 10, 2022, from https://richardturton.faculty.wvu.edu/publications/analysis-synthesis-and-design-of-chemical-processes-5th-edition.

Turton, R., Bailie, R. C., Whiting, W. B., Shaeiwitz, J. A., & Bhattacharyya, D. (2016). Chapter 8. Estimation of Manufacturing Costs. In *Analysis, Synthesis, and Design of Chemical Processes, Fourth Edition* (4th ed.). story, Pearson India Education Services.

Twiford, R. J. (2022, January 31). *How to Calculate Transmembrane Pressure*. Membrane System Specialists, Inc. Retrieved March 4, 2022, from https://www.mssincorporated.com/blog/how-to-calculate-transmembrane-

pressure/#:~:text=Transmembrane%20pressure%20is%20the%20amount,concentration%20polarization%20and%20membrane%20fouling.

Tzanetis, K. F., Posada, J. A., & Ramirez, A. (2017). Analysis of biomass hydrothermal liquefaction and bio-crudeoil upgrading for renewable jet fuel production: The impact of reaction conditions on production costs and GHG emissions performance. *Renewable energy*, *113*, 1388-1398.

ULINE. (n.d.). CLR® Calcium, Lime and Rust Remover. ULINE. Retrieved April 6, 2022, from https://www.uline.com/BL_7097/CLR-Calcium-Lime-and-Rust-Remover?pricode=WU409&AdKeyword=clr+cleaning+products&AdMatchtype=p&gclid=CjwKCAjw0a-SBhBkEiwApljU0oNCI7rBhywMMmozQDPssZ5nJgGl9QRQsC2EB2Do79xo2dyXd3nPARoCIUoQAvD_BwE&gclsrc=aw.ds

U.S. Environmental Protection Agency. (n.d.). *Operation & Maintenance Checklist and Tasks*. Retrieved April 8, 2022, from https://www.epa.gov/sites/default/files/documents/om_checklisttasks.pdf.

Varadhan, S. (2019, June 20). Hotels, companies cut back on water use as taps run dry in Chennai. Business Standard. Retrieved February 14, 2022, from https://www.business-standard.com/article/current-affairs/hotels-companies-cut-back-on-water-use-as-taps-run-dry-in-chennai-119061900873_1.html.

Vitasalus. (2021). Inline Ultraviolet Water Disinfection System. Inline UV - inline ultraviolet water disinfection system. Retrieved April 1, 2022, from http://www.equinox-products.com/InlineUV.htm

Voutchkov, N. (2005). Settling Tanks. Water Encyclopedia. https://doi.org/10.1002/047147844x.mw506

Wateranywhere. (2021). *8"x40": 7,500 GPD: 99.8% rejection: Filmtec Seawater Membrane*. SW30HRLE-400. Retrieved February 14, 2022, from https://wateranywhere.com/8-x40-7-500-gpd-99-8-rejection-filmtec-seawater-membrane/

Wateranywhere. (2021). *8"x40": 10,500 GPD: 99.5% REJ: 400 FT2: Filmtec RO membrane.* BW30-400. Retrieved February 15, 2022, from https://wateranywhere.com/8-x40-10-500-gpd-99-5-rej-400-ft2-filmtec-ro-membrane/#:~:text=Specifications%20for%20BW30-400%20Permeate%20flow%20and%20salt%20rejection,for%20continuous%20operation%20above%20pH%2010%20is%2095%C2%B0F.

Yu, F., Zhou, G., Xu, J., & Ge, W. (2015). Enhanced axial mixing of rotating drums with alternately arranged baffles. *Powder Technology, 286*, 276-287.